

# Impact of Nuclear Reaction Rate Uncertainties on Type I X-ray Burst Nucleosynthesis: A Monte Carlo Study

QING WANG<sup>1</sup>,<sup>2</sup> ERTAO LI<sup>1</sup>,<sup>2</sup> ZHIHONG LI<sup>1</sup>,<sup>2</sup> YUBAO WANG<sup>1</sup>,<sup>2</sup> BING GUO<sup>1</sup>,<sup>2</sup> YUNJU LI<sup>1</sup>,<sup>2</sup> JUN SU<sup>1</sup>,<sup>3</sup>  
SHIPENG HU<sup>1</sup>,<sup>2</sup> YINWEN GUAN<sup>1</sup>,<sup>2</sup> DONG XIANG<sup>1</sup>,<sup>2</sup> YU LIU<sup>1</sup>,<sup>2</sup> LEI YANG<sup>1</sup>,<sup>2</sup> AND WEIPING LIU<sup>1</sup>,<sup>2</sup>

<sup>1</sup>Shenzhen Key Laboratory of Research and Manufacture of High Purity Germanium Materials and Detectors, Institute for Advanced Study in Nuclear Energy & Safety, College of Physics and Optoelectronic Engineering, Shenzhen University, Shenzhen 518060, Guangdong, People's Republic of China

<sup>2</sup>China Institute of Atomic Energy, Beijing 102413, People's Republic of China

<sup>3</sup>School of Physics and Astronomy, Beijing Normal University, Beijing 100875, People's Republic of China

<sup>4</sup>Department of Physics, Southern University of Science and Technology, Shenzhen 518055, Guangdong, People's Republic of China

## ABSTRACT

To investigate the impact of nuclear reaction rate uncertainties on type I X-ray burst nucleosynthesis, comprehensive Monte Carlo simulations are performed with temperature-independent and -dependent variations in reaction rates using the REACLIB and STARLIB libraries, respectively. A total of 1,711 ( $p, \gamma$ ), ( $p, \alpha$ ), ( $\alpha, p$ ), and ( $\alpha, \gamma$ ) reactions are varied simultaneously, along with their inverse reactions, via detailed balance. For the first time, it is found that Monte Carlo sampling with larger perturbations to these reaction rates may lead to multi-peaked abundance distributions for some isotopes. These multi-peak structures arise not only from coupled reactions but also, in some cases, from single reactions. Our study also confirmed previously identified key reactions and provides more robust lists. These reactions deserve priority consideration in future study.

**Keywords:** Monte Carlo, Nuclear reaction rate, Abundance, Type I X-ray burst, Nucleosynthesis

## 1. INTRODUCTION

Type I X-ray bursts (XRBs) are the most frequent thermonuclear explosions observed in our Galaxy (R. H. Cyburt et al. 2016; A. Parikh et al. 2013). They are powered by unstable hydrogen and helium burning on the accreted envelope of neutron stars in low-mass X-ray binary systems (LMXBs) (C. J. Hansen et al. 1975; S. E. Woosley & R. E. Taam 1976; P. C. Joss 1977; R. H. Cyburt et al. 2010). In the regime of combined H/He ignition, XRBs are dominated by  $3\alpha$  reaction,  $\alpha p$ -process (a suite of ( $\alpha, p$ ) and ( $p, \gamma$ ) reactions) and  $rp$ -process (a sequence of rapid proton captures and  $\beta^+$  decays) (J. L. Fisker et al. 2008; R. K. Wallace et al. 1981; S. E. Woosley et al. 2004; H. Schatz et al. 2001; J. José et al. 2010; A. Parikh et al. 2013). Under the most favorable conditions (high hydrogen content in the accreted matter, low metallicity, and high accretion rate), reactions can proceed up to and terminate in the SnS-bTe cycle (H. Schatz et al. 2001; R. H. Cyburt et al. 2010). These nuclear processes involve hundreds of nuclear species from stable isotopes to the proton drip line. Thousands of nuclear reactions have not been determined experimentally with large uncertainties (R. H. Cyburt et al. 2016). To explore these uncertainties on

XBR models, extensive investigations have been conducted.

Varying reaction rates individually is a classical method to quantify the numerical sensitivity of observables to specific reactions (H. Schatz 2016) on XRB models. In particular, R. H. Cyburt et al. (2016) investigated the impact of uncertainties in ( $p, \gamma$ ), ( $\alpha, \gamma$ ), and ( $\alpha, p$ ) nuclear reaction rates by varying each reaction rate individually, first screening sensitive reactions in onezone model and then recalculating the important ones in fully self-consistent 1D multizone model. They found a number of reactions that significantly affect the predictions of light curves and burst ashes. Y. H. Lam et al. (2022a) carried out a sensitivity study of individual reactions to examine their influence on photospheric radius expansion of X-ray bursts, and found that the observables are more sensitive to some  $\alpha$ -capture reactions.

Nevertheless, it has been claimed (L. F. Roberts et al. 2006) that due to many different channels are coupled in nucleosynthesis, traditional sensitivity studies, in which only one reaction is varied while the others are held constant, cannot adequately address all the important correlations and may lead to wrong (or at least biased) conclusions. Monte Carlo studies have the advantage that they take into account all correlations between reactions and that they can be used to properly propagate uncertainties quantitatively to the predicted observables (H.

Schatz 2016). It have already been performed for several other astrophysical scenarios: Big Bang Nucleosynthesis (BBN) (C. Iliadis & A. Coc 2020),  $\nu p$ -process (N. Nishimura et al. 2019),  $s$ -process (G. Cescutti et al. 2018),  $r$ -process (M. R. Mumpower et al. 2016), weak  $r$ -process (J. Bliss et al. 2020; A. Psaltis et al. 2022),  $i$ -process (P. A. Denissenkov et al. 2021),  $\gamma$ -process (T. Rauscher et al. 2016), weak  $rp$ -process (A. Psaltis et al. 2025), AGB stars (C. E. Fields et al. 2016) and Massive stars (C. E. Fields et al. 2018). For XRBs, A. Parikh et al. (2008) systematically varied 3,500 nuclear reactions individually and simultaneously based on temperature and density profiles using onezone post-processing models.

In some of these and similar studies like A. Parikh et al. (2008), temperature-independent estimates of the reaction rate uncertainties were applied as constant multiplicative factors on the recommended rates at all temperatures (hereafter a temperature-independent Monte Carlo method), which may lead to either an underestimation or an overestimation of the reaction rate at different stellar temperatures (C. E. Fields et al. 2016, 2018). However, R. Longland (2012) demonstrated that this method provides a reasonable approximation to theoretical rates and has been adopted in subsequent studies of the weak  $r$ -process, e.g., J. Bliss et al. (2020) and A. Psaltis et al. (2022).

In reality, the uncertainties of individual reaction rates are often temperature-dependent when based on experimental constraints, usually with larger uncertainties at lower temperatures. For XRB nucleosynthesis, although most reaction rates are calculated using theoretical models, some key reactions are experimentally determined. Each reaction rate carries its own uncertainty, and using realistic uncertainties for all rates is essential in Monte Carlo simulations; otherwise, the simultaneous variation of all reactions may lead to unreasonable results (A. Parikh et al. 2008). A more robust approach incorporates temperature-dependent uncertainties, as provided by the STARLIB library (A. L. Sallaska et al. 2013), which enables Monte Carlo simulations for more realistic nucleosynthesis calculations (hereafter a temperature-dependent Monte Carlo method; see also R. Longland 2012; C. E. Fields et al. 2016, 2018; A. Psaltis et al. 2025).

Classical reaction rates are often reported with sharp upper and lower limits, lacking a rigorous statistical meaning (R. Longland et al. 2010). For instance, the NACRE evaluation (C. Angulo et al. 1999) provides recommended, lower and upper rates as fixed boundaries, without specifying any coverage probability. In contrast, STARLIB (R. Longland et al. 2010; A. L. Sallaska et al. 2013) employs a Monte Carlo framework in which reaction rate uncertainties are characterized by lognormal probability distributions, and the reported uncertainties correspond to a 68.3% coverage probability. For those reactions with no experimental data avail-

able, the STARLIB library assigned a factor uncertainty ( $f.u.$ ) of 10 over entire temperature (A. L. Sallaska et al. 2013; A. Psaltis et al. 2025), based on theoretical statistical Hauser–Feshbach model. A. Parikh et al. (2008) and J. Bliss et al. (2020) assumed that all considered reaction rates have an uncertainty of roughly a factor of ten, but adopted different coverage probabilities (95.5% and 68.3%, respectively), using the temperature-independent Monte Carlo method, which may lead to significant differences in predicting final abundances and identifying key reactions.

To date, no systematic investigations have been performed to examine the influence of coverage probabilities. To fill this gap, this work provides a self-consistent study that explores the effects of different coverage probabilities on the final abundances and the identification of key reactions using the temperature-independent Monte Carlo method. We further quantify the effects of reaction rate uncertainties using the temperature-dependent Monte Carlo method in STARLIB. This study aims to provide insights for future Monte Carlo simulations and nuclear reaction rates, theoretically and experimentally.

This paper is organized as follows: Section 2 provides a detailed description of the models and methods employed in our study. In Section 3, we present the results of our simulations. Finally, Section 4 discusses the implications of our findings and draws conclusions.

## 2. MODELS AND METHODS

### 2.1. Models: Temperature and Density profiles

We employed three different XRB Models K04 (O. Koike et al. 2004), S01 (H. Schatz et al. 2001), and S16 (R. H. Cyburt et al. 2016). Their temperature and density profiles can be seen from Figure 1.

Model K04 has a peak temperature of 1.36 GK, densities ranging from 0.54 to  $1.44 \times 10^6$  g/cm<sup>3</sup>, and a burst duration of approximately 100 s. Its initial composition follows A. Parikh et al. (2008) (based on O. Koike et al. (2004)), with  $X = 0.73$ ,  $Y = 0.25$ , and  $Z = 0.02$ , where  $Z$  is scaled according to the solar abundances (N. Grevesse et al. 1998).

Model S01 has the highest peak temperature among the considered models, with  $T_{\text{peak}} = 1.907$  GK and lasts for about 300 s. Unlike previous studies (A. Parikh et al. 2008) that scaled densities from K04, we adopt the actual density profile for this model. The initial composition is  $X = 0.718$ ,  $Y = 0.281$ , and  $Z = 0.001$ . Following A. Parikh et al. (2008), we assume that all metals are initially in the form of  $^{14}\text{N}$ , as described by S. E. Woosley et al. (2004).

Model S16 represents a burst characterized by a lower peak temperature of  $T_{\text{peak}} = 1.2$  GK. The trajectory was calculated using the onezone model. Its ignition conditions were chosen from the multi-zone model so that the resulting luminosity and final composition closely resemble those of the multi-zone calculation. The selected ignition conditions correspond to a temperature of 0.386

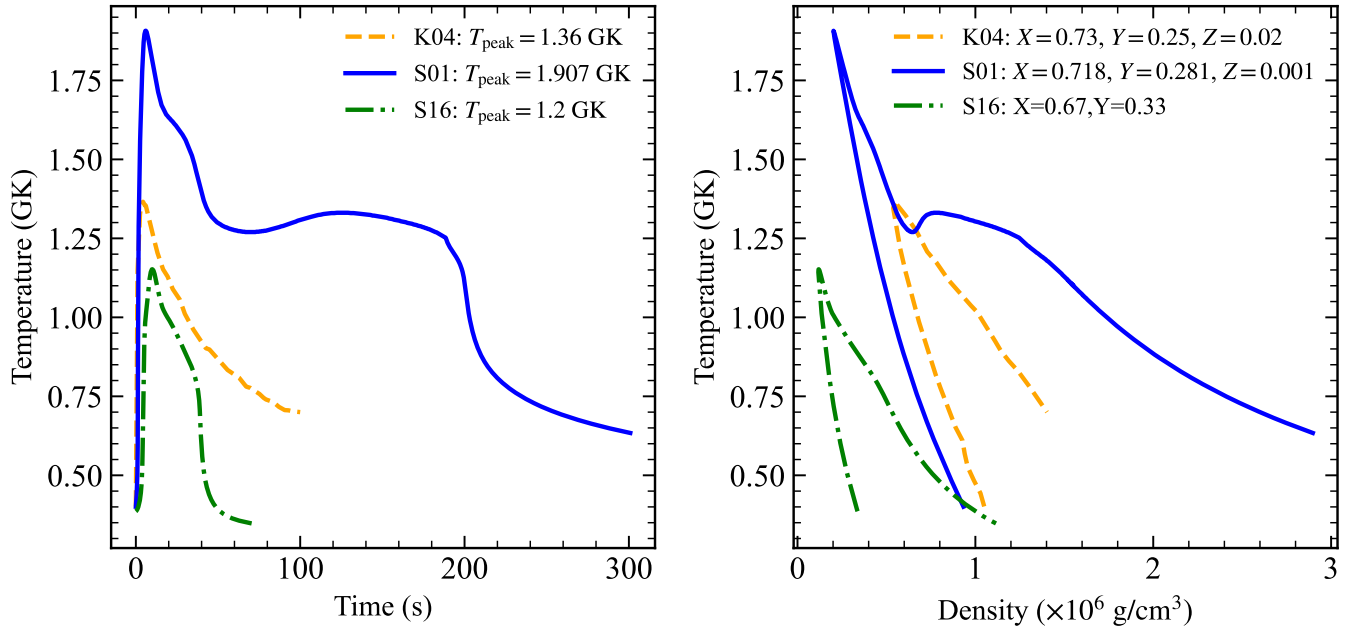


**Figure 1.** (Left) Time evolution of temperature for the XRB Models K04 (orange dashed line) (O. Koike et al. 2004), S01 (blue solid line) (H. Schatz et al. 2001), and S16 (green dot-dashed line) (R. H. Cyburt et al. 2016). (Right) Same as left panel, but for temperature vs. density (in units of  $10^6$  g/cm<sup>3</sup>). The peak temperature and initial metallicity for each model are listed as well.

GK, a pressure of  $1.73 \times 10^{22}$  ergs/cm<sup>3</sup>, and hydrogen and helium mass fractions of 0.51 and 0.39, respectively, as reported by R. H. Cyburt et al. (2016). Instead of using  $X = 0.51$  and  $Y = 0.39$  as the initial composition in this work, we adopted  $X = 0.67$  and  $Y = 0.33$ , following M. Zhang et al. (2024) with zero metallicity, taken from H. Schatz et al. (2001).

## 2.2. Nucleosynthesis Methods

Nucleosynthesis studies of XRBs are computationally challenging due to short characteristic timescales and high peak temperatures. The large number of nuclear species and extensive reaction networks (several thousand nuclear processes) required to describe the  $rp$ -process and  $\alpha p$ -process in H- and He-rich mixtures accreted onto the surface of a neutron star further increase the computational complexity. Since full reaction networks coupled to multizone hydrodynamic models remain computationally prohibitive (A. Parikh et al. 2013), onezone post-processing (A. Parikh et al. 2008) or onezone (R. H. Cyburt et al. 2016) calculations are often adopted as practical alternatives for comprehensive studies.

In this work, the onezone post-processing method was adopted using the WinNet code. The network consists of 686 nuclides, from hydrogen to <sup>136</sup>Xe, and includes more than 8,000 reactions. Among these, 1,711 forward reactions—( $p, \gamma$ ), ( $p, \alpha$ ), ( $\alpha, p$ ) and ( $\alpha, \gamma$ )—were varied, and the corresponding inverse rates were calculated via detailed balance, whereas all other reactions

remained unchanged and were adopted from REACLIB v2.2 (R. H. Cyburt et al. 2010). For the temperature-independent Monte Carlo method, these reactions were randomly sampled using lognormal multiplicative factors around their REACLIB median (recommended) rates. For the temperature-dependent Monte Carlo method, they followed the median rates and associated uncertainties from STARLIB v610 (A. L. Sallaska et al. 2013). Thus, each of the reactions was independently perturbed according to a lognormal distribution based on its REACLIB or STARLIB rate. A detailed description of the sampling procedure is presented in Section 2.3.

Although A. Parikh et al. (2008) performed preliminary Monte Carlo studies with 1,000 trials and found that increasing the number of trials to 10,000 did not reveal additional correlations, we further extended our simulations to 100,000 trials per model and run. This allows investigation of rare tail events and improves statistical reliability.

## 2.3. Monte Carlo Sampling Methods

### 2.3.1. Temperature-Independent Monte Carlo Method

A lognormal distribution can approximately describe the probability density function of reaction rates. In each Monte Carlo trial  $i$ , a reaction rate is independently scaled by a random multiplicative factor,  $p$ , applied consistently across all temperature points:

$$r_i = r_{\text{med}} \times p, \quad (1)$$

where  $r_{\text{med}}$  is the median rate adopted from REACLIB.  $p$  follows a lognormal probability density function.

$$f(p) = \frac{1}{\sqrt{2\pi}\sigma p} e^{-(\ln(p)-\mu)^2/(2\sigma^2)}, \text{ for } 0 < p < \infty. \quad (2)$$

The parameters  $\mu$  and  $\sigma$  represent the mean value and standard deviation of the Gaussian distribution for  $\ln(p)$ . In each Monte Carlo trial, all reaction rates are varied simultaneously within their respective uncertainties.

As previously described, A. Parikh et al. (2008) and J. Bliss et al. (2020) assumed that all rates considered have an uncertainty of roughly a factor of ten, but adopted different coverage probabilities and parameters. Specifically, A. Parikh et al. (2008) used  $\mu = 0$  and  $\sigma = 1.15$ , corresponding to a 95.5% coverage probability ( $2\sigma$ ). In contrast, J. Bliss et al. (2020) used  $\mu = 0$  and  $\sigma = 2.3$ , corresponding to a 68.3% coverage probability ( $1\sigma$ ). This choice represents a broader distribution in the Monte Carlo samples, leading to larger perturbations in the reaction rates. To assess the impact of these differences on final abundances and the identification of key reactions, both sets of lognormal parameters ( $\sigma = 1.15$  and  $\sigma = 2.3$ ) were employed. The results are presented in Section 3.1.

### 2.3.2. Temperature-Dependent Monte Carlo Method

The STARLIB rate library provides the median nuclear reaction rate,  $r_{\text{med}}$ , and the associated factor uncertainty,  $f.u.$  (for a 68% coverage probability), at temperature ranges from 0.001 GK to 10 GK (A. L. Sallaska et al. 2013). All rates in STARLIB also follow a lognormal probability distribution at each temperature  $T$ .

$$f(r) = \frac{1}{\sqrt{2\pi}\sigma r} e^{-(\ln(r)-\mu)^2/(2\sigma^2)}, \text{ for } 0 < r < \infty, \quad (3)$$

where  $r$  is the reaction rate. The lognormal function has two parameters  $\mu$  and  $\sigma$ . Following R. Longland et al. (2010); A. L. Sallaska et al. (2013),  $r_{\text{med}}$  is related to the location parameter  $\mu$ ,  $r_{\text{med}} = e^\mu$ .  $f.u.$  is related to the spread parameter  $\sigma$ ,  $f.u. = e^\sigma$ .

In each Monte Carlo trial  $i$ , a random variation factor  $p_{ij}$  is assigned to each reaction rate (R. Longland 2012; A. L. Sallaska et al. 2013; C. E. Fields et al. 2016):

$$r_{ij} = e^\mu (e^\sigma)^{p_{ij}} = r_{\text{med}} (f.u.)^{p_{ij}}, \quad (4)$$

where  $p_{ij}$  is drawn from a normal distribution with a mean of zero and standard deviation of unity for the  $j$ -th sampled reaction rate. When the rate variation factor  $p_{ij} = 0$ , the median rate  $r_{\text{med}}$  can be recovered. Since the factor uncertainty  $f.u.$  varies with temperature, a sampled rate distribution maintains the temperature dependence of the rate uncertainty. For a more detailed discussion of the sampling procedure used in

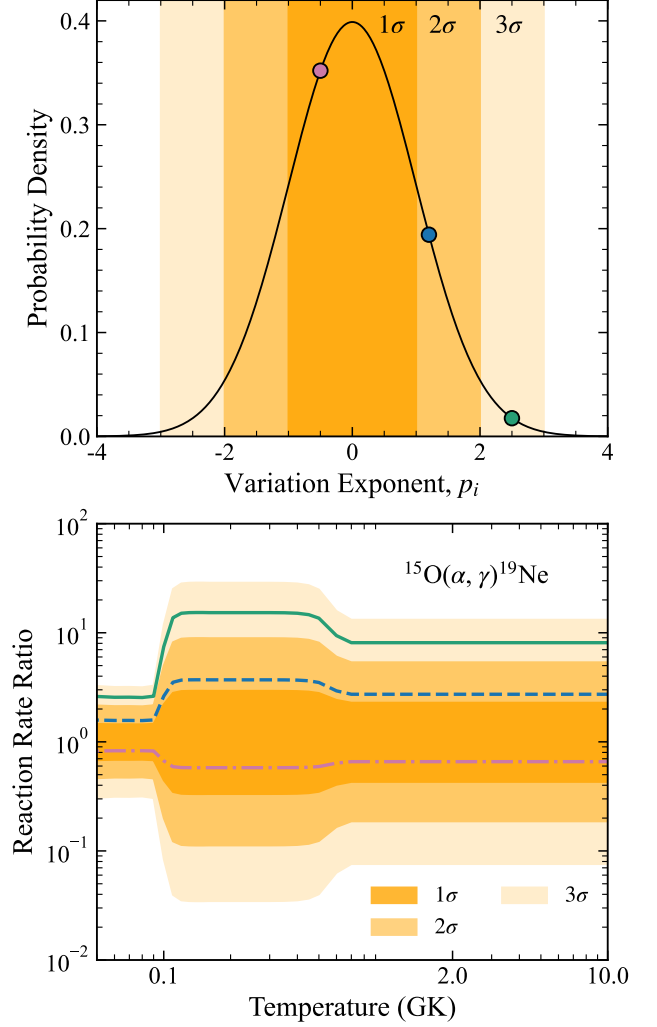


**Figure 2.** (Top) Standard normal distribution of reaction rate variation factor  $p_i$ . three points of  $p_i = -0.5, 1.2$ , and  $2.5$  are also drawn from left to right. (Bottom) The resulting reaction rates compared to the median for the  $^{15}\text{O}(\alpha, \gamma)^{19}\text{Ne}$  reaction rate. In the bottom panel, these points are mapped to reaction rates according to Equation 4, and then compared with the median, corresponding to the red dot-dashed, blue dashed, and green solid lines, respectively.

Monte Carlo nucleosynthesis studies, the reader is referred to R. Longland (2012).

Following (A. Psaltis et al. 2025), we illustrate the above sampling procedure in Figure 2 using the example of  $^{15}\text{O}(\alpha, \gamma)^{19}\text{Ne}$ . In the top panel, the violet, blue, and green points correspond to three rate variation factors,  $p_i = -0.5, 1.2$ , and  $2.5$ , drawn from the standard normal distribution. In the bottom panel, these points are mapped to reaction rates using Equation 4 and then compared with the median, represented by the violet dot-dashed, blue dashed, and green solid lines, respectively.



The reaction rate ratio is not constant but follows the temperature dependence of the rate uncertainty.

#### 2.4. Identification of Key Reactions

In both temperature-dependent and temperature-independent Monte Carlo simulations, the impact of reaction rate uncertainties on final abundances of isotopes can be calculated using correlation coefficients. Previous studies employed the Pearson correlation coefficient to capture linear relationships (N. Nishimura et al. 2019; T. Rauscher et al. 2016), while the Spearman rank-order correlation (SROC) captures monotonic trends, including nonlinear ones (C. E. Fields et al. 2016, 2018; J. Bliss et al. 2020; A. Psaltis et al. 2022). More recently, mutual information (MI) has been introduced to quantify correlations that are neither linear nor monotonic (C. Iliadis & A. Coc 2020; A. Psaltis et al. 2025). In this work, we focus on SROC, as it provides a clear measure of both the strength and direction of these monotonic dependencies.

For the  $J = 1711$  reactions, each reaction has  $N = 10^5$  pre-generated Monte Carlo samples, forming the matrix  $p = \{p_{ij}\} \in \mathbb{R}^{N \times J}$ , with the corresponding final abundances of isotopes  $X = \{x_{ik}\} \in \mathbb{R}^{N \times K}$ .

Each column of  $p$  and  $X$  is replaced by its rank values, resulting in the matrices  $p_{\text{rank}} \in \mathbb{R}^{N \times J}$  and  $X_{\text{rank}} \in \mathbb{R}^{N \times K}$ . Each ranked column is then standardized using its column-wise mean and sample standard deviation:

$$\tilde{p} = \frac{p_{\text{rank}} - \bar{p}}{s_p}, \quad \tilde{X} = \frac{X_{\text{rank}} - \bar{X}}{s_X}, \quad (5)$$

where  $\bar{p}$  and  $\bar{X}$  denote the column-wise means, and  $s_p$  and  $s_X$  are the corresponding standard deviations. The Spearman rank correlation matrix  $R_s \in \mathbb{R}^{J \times K}$  is obtained as

$$R_s = \frac{\tilde{p}^\top \tilde{X}}{N - 1}. \quad (6)$$

The  $(j, k)$  element of the matrix  $R_s$  represents the Spearman correlation coefficient, denoted as  $r_s$ , between the  $j$ -th reaction and the  $k$ -th isotope. A value of  $r_s = +1$  indicates a perfectly monotonically increasing relationship, while  $r_s = 0$  signifies no correlation at all. Conversely,  $r_s = -1$  indicates a perfectly monotonically decreasing relationship. We have confirmed that these results align with those obtained using the `scipy.stats.spearmanr` function (P. Virtanen et al. 2020), following time-consuming loop calculations for all pairs of isotopes and reactions.

The Spearman correlation coefficients alone are insufficient for identifying the most important reactions of a given isotope, as they do not account for the extent of abundance variations (A. Parikh et al. 2008; J. Bliss et al. 2020). Therefore, we identified key reactions by simultaneously considering both the variations in isotopic abundances and the associated Spearman correlation coefficients.

### 3. RESULTS

In this section, we present the main results from Monte Carlo simulations carried out with the WinNet code (C. Winteler et al. 2012; M. Reichert et al. 2023). After the completion of each trajectory, all radioactive species with half-lives shorter than 1 h were allowed to decay into their respective stable daughter nuclides, following A. Parikh et al. (2008); A. Psaltis et al. (2025).

This work aims at identifying key reactions whose uncertainties strongly influence nucleosynthetic predictions. Instead of using absolute yields, we considered relative abundances, i.e., abundances from the Monte Carlo trials normalized to baseline abundances. For the temperature-independent Monte Carlo simulations, REACLIB v2.2 was used to calculate baseline abundances  $X_{\text{base}}$  for each model. For the temperature-dependent simulations, REACLIB v2.2, with the 1,711 forward rates replaced by the median rates from STARBIB v610, was used to compute  $X_{\text{base}}$  for each model. Inverse reaction rates were also calculated using detailed balance.

#### 3.1. Temperature-Independent Monte Carlo Simulations

Since the analysis methods are similar across all models and to limit the scope of this work, we focus on discussing the results for Model K04 in the following section.

As illustrated in Figure 3, there is a strong correlation between the normalized abundance of  $^{69}\text{Ge}$  and  $^{69}\text{Se}(p, \gamma)^{70}\text{Br}$  for both  $\sigma = 1.15$  and  $\sigma = 2.3$ . The absolute Spearman coefficient  $|r_s|$  is larger for  $\sigma = 1.15$  than for  $\sigma = 2.3$ , whereas the corresponding abundance uncertainty is larger in the latter case (see also Table 2). In particular, Figure 3(b) highlights a more significant variability in the relative abundance of  $^{69}\text{Ge}$ , with numerous discrete points distributed on both sides of the central area. Figure 3(a) is consistent with Fig. 8 of A. Parikh et al. (2008), who reported a correlation coefficient of  $-0.972$  between the abundance of  $^{69}\text{Ge}$  and  $^{69}\text{Se}(p, \gamma)^{70}\text{Br}$ . Compared to their 1,000 Monte Carlo simulations, which show some discrete points, our 100,000 simulations reveal a clearer clustering of discrete points.

When it comes to the distribution of relative abundances, F. Moreno & J. José (2009) showed that distributions are close to normal for some isotopes with small uncertainties (i.e.,  $^{41}\text{Ca}$  and  $^{46}\text{Ti}$ ), whereas isotopes (isotopic relative abundances) with larger uncertainties (i.e.,  $^{15}\text{N}$  and  $^{60}\text{Ni}$ ) follow a lognormal distribution. Our analysis on a logarithmic scale indicates that the distributions of relative abundances generally approximate normal or lognormal distributions. For  $\sigma = 2.3$ , certain isotopes (isotopic relative abundances on a logarithmic scale), however, exhibit multi-peaked structures, such as  $^{55}\text{Co}$ , as shown in Figure 4(b); in contrast, for  $\sigma = 1.15$ , no multi-peaked structures were

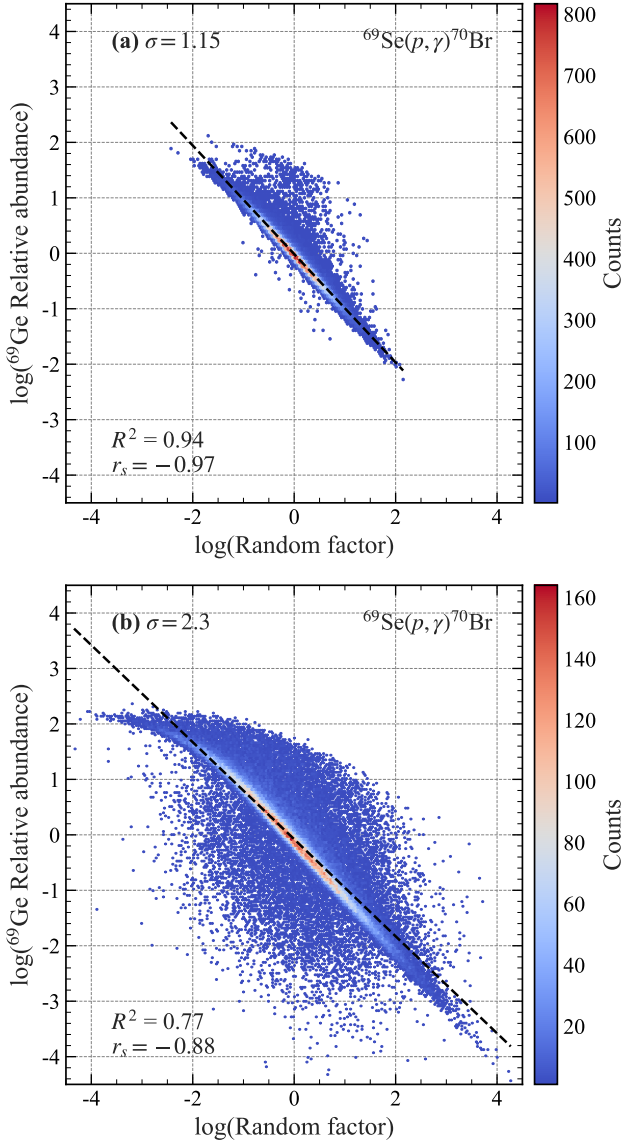


**Figure 3.** Effect of  $^{69}\text{Se}(p, \gamma)^{70}\text{Br}$  rate variations on the normalized abundance of  $^{69}\text{Ge}$  in Model K04. The reaction shows a strong negative correlation with  $^{69}\text{Ge}$ . Compared to  $\sigma = 1.15$ , the linear regression  $R^2$  (black dashed line) and absolute Spearman correlation coefficient  $|r_s|$  are smaller for  $\sigma = 2.3$ , while the corresponding abundance uncertainty is larger.

observed. To investigate the origin of the multi-peaked structure of  $^{55}\text{Co}$  for  $\sigma = 2.3$ , our correlation analysis identifies four reactions as the main contributors to its abundance pattern:  $^{55}\text{Ni}(p, \gamma)^{56}\text{Cu}$  ( $r_s = -0.39$ ),  $^{56}\text{Cu}(p, \gamma)^{57}\text{Zn}$  ( $r_s = -0.43$ ),  $^{59}\text{Cu}(p, \alpha)^{56}\text{Ni}$  ( $r_s = 0.23$ ) and  $^{59}\text{Cu}(p, \gamma)^{60}\text{Zn}$  ( $r_s = -0.23$ ).

As shown in Figure 5, the abundances of  $^{55}\text{Co}$  form two distinct clusters, separated by the value corresponding to the minimum probability density between the two peaks, as shown in Figure 4(b). Within the primary

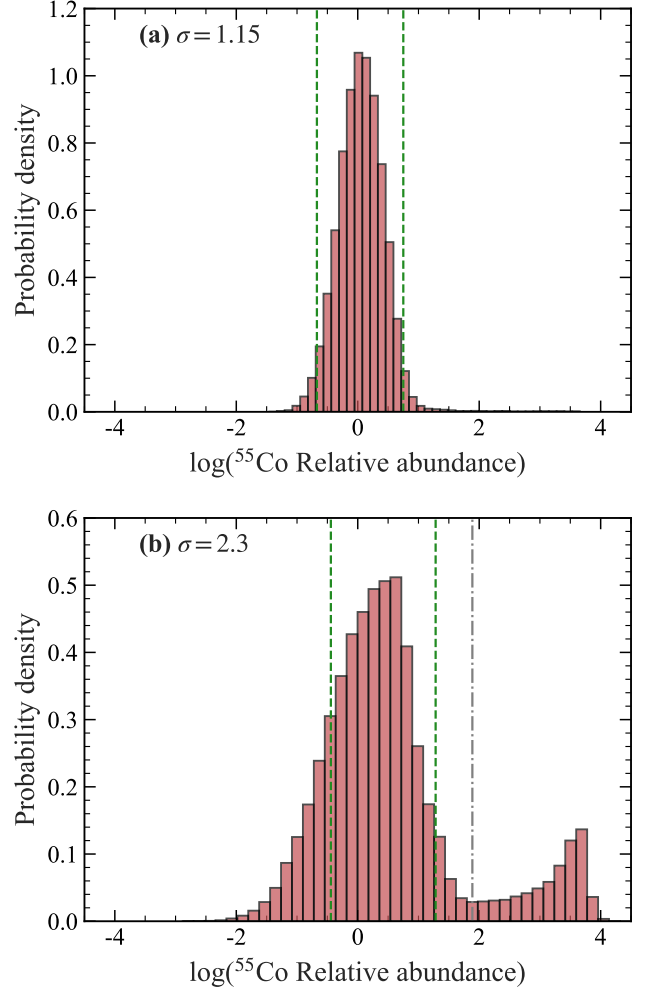


**Figure 4.** Histogram of the logarithmic relative abundances of  $^{55}\text{Co}$  in Model K04. The green dashed lines indicate the 95% (2.5<sup>th</sup>–97.5<sup>th</sup> percentile) and 68% (16<sup>th</sup>–84<sup>th</sup> percentile) confidence intervals (C.I.s) in the top and bottom panels, respectively. The gray dot-dashed line in the bottom panel denotes the location of minimum probability density between the two peaks.

clusters (Figure 5a–b), the abundance of  $^{55}\text{Co}$  shows stronger correlations with  $^{55}\text{Ni}(p, \gamma)^{56}\text{Cu}$  ( $r_s = -0.51$ ) and  $^{56}\text{Cu}(p, \gamma)^{57}\text{Zn}$  ( $r_s = -0.55$ ) compared to the global cluster ( $r_s = -0.39$  and  $r_s = -0.43$ ), whereas correlations in the secondary clusters are weak. In contrast, within the secondary clusters (Figure 5c–d),  $^{55}\text{Co}$  exhibits slightly stronger correlations with  $^{59}\text{Cu}(p, \alpha)^{56}\text{Ni}$  ( $r_s = 0.28$ ) and  $^{59}\text{Cu}(p, \gamma)^{60}\text{Zn}$  ( $r_s = -0.27$ ) than in the global cluster ( $r_s = 0.23$  and  $r_s = -0.23$ ), while correlations in the primary clusters remain weak.

Figure 6(b) further confirms that the bimodal distribution of  $^{55}\text{Co}$  mainly arises from the competition between  $^{59}\text{Cu}(p, \gamma)^{60}\text{Zn}$  and  $^{59}\text{Cu}(p, \alpha)^{56}\text{Ni}$ . The ratio of the assigned variation factors clearly separates tri-

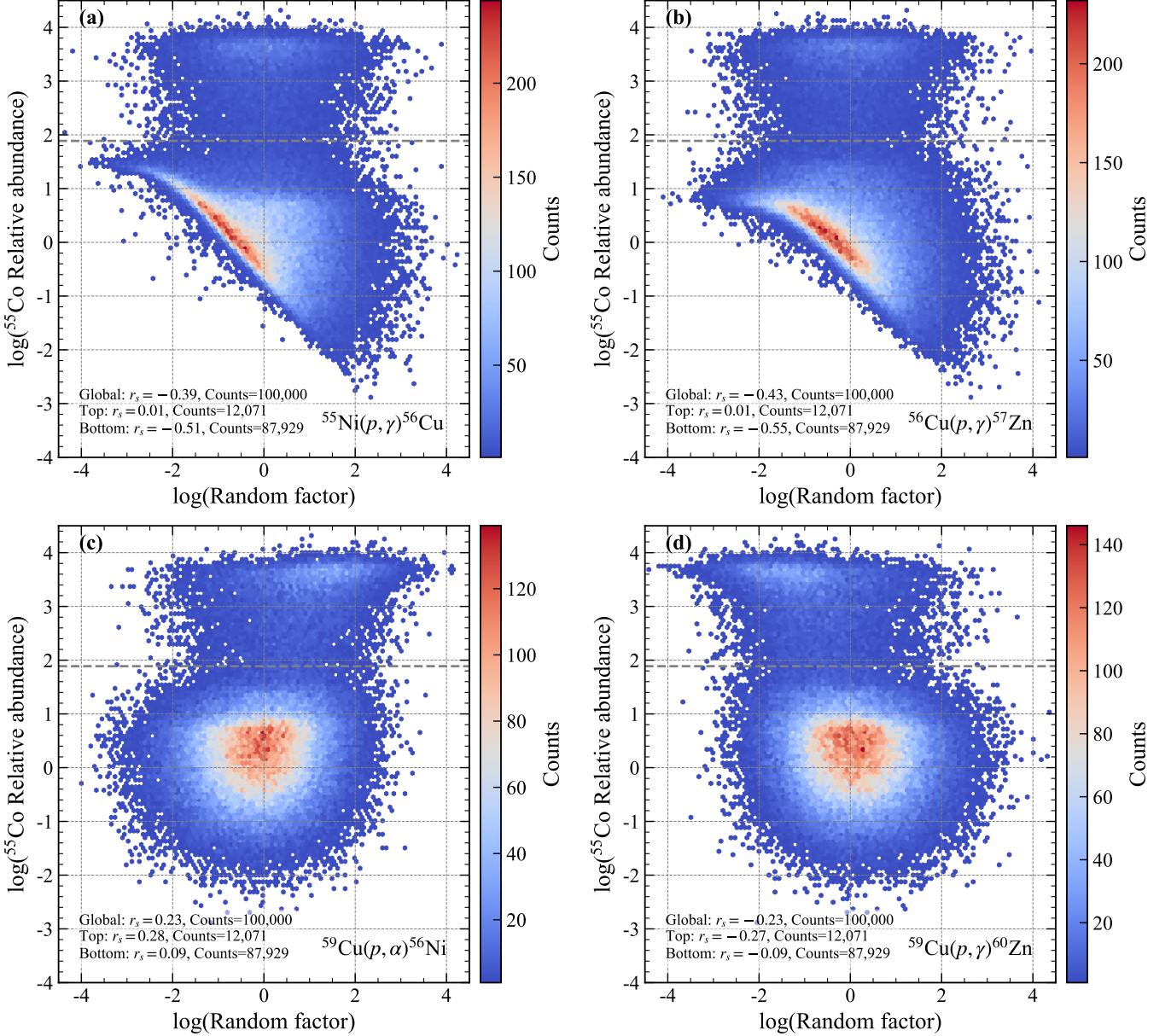


**Figure 5.** Similar to Figure 3, but for the correlations between the abundance of  $^{55}\text{Co}$  and the reactions (a)  $^{55}\text{Ni}(p, \gamma)^{56}\text{Cu}$ , (b)  $^{56}\text{Cu}(p, \gamma)^{57}\text{Zn}$ , (c)  $^{59}\text{Cu}(p, \alpha)^{56}\text{Ni}$ , and (d)  $^{59}\text{Cu}(p, \gamma)^{60}\text{Zn}$  in Model K04 with  $\sigma = 2.3$ . Gray dashed lines separate the primary (bottom) and secondary (top) clusters, corresponding to the minimum of the probability density of  $^{55}\text{Co}$  indicated by the gray dot-dashed line in Figure 4(b). Each cluster is analyzed individually, with the Spearman correlation coefficient ( $r_s$ ) and sample counts reported at the bottom of each panel.

als leading to the high- and low-abundance peaks. For  $\sigma = 1.15$  (Figure 6(a)), the  $^{55}\text{Co}$  distribution remains single-peaked with a slight tail. The observed separation originates from the competition between the  $p$ -capture and  $\alpha$ -capture on  $^{59}\text{Cu}$ . When the ratio exceeds a threshold, an alternative abundance pattern can emerge, becoming increasingly likely with larger Monte Carlo perturbations.

Figure 7 presents the integrated net fluxes (currents) in the NiCu region. Figure 7(a) shows the fluxes under

standard reaction rates, while Figure 7(b) depicts the case of a representative Monte Carlo trial for  $\sigma = 2.3$ , in which the randomly sampled ratio  $^{59}\text{Cu}(p, \alpha)^{56}\text{Ni} / ^{59}\text{Cu}(p, \gamma)^{60}\text{Zn}$  exceeds 100, indicating a strong preference for the  $(p, \alpha)$  channel. The enhanced  $(p, \alpha)$  flow strengthens the NiCu cycle, thereby accelerating hydrogen consumption and reducing the flow toward heavier Zn isotopes, which leads to the bimodal abundance distribution of  $^{55}\text{Co}$ . However, the abundance of  $^{55}\text{Co}$  shows weak correlations with  $^{59}\text{Cu}(p, \alpha)^{56}\text{Ni}$  and

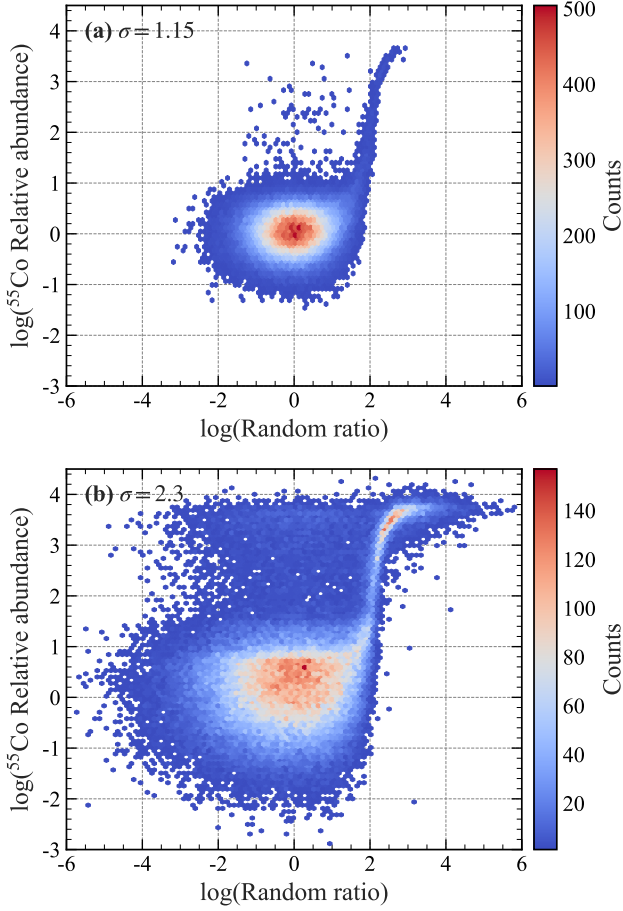


**Figure 6.** Effect of the variation factor ratio,  $^{59}\text{Cu}(p, \alpha)^{56}\text{Ni} / ^{59}\text{Cu}(p, \gamma)^{60}\text{Zn}$ , on the abundance of  $^{55}\text{Co}$  in Model K04. (a)  $\sigma = 1.15$ : the distribution of  $^{55}\text{Co}$  remains single-peaked with a slight tail. (b)  $\sigma = 2.3$ : the ratio clearly separates trials leading to the high- and low-abundance peaks, illustrating the formation of the bimodal distribution.

$^{59}\text{Cu}(p, \gamma)^{60}\text{Zn}$ , as indicated by the Spearman correlation coefficients. These results highlight the sensitivity of isotopic abundances to the  $^{59}\text{Cu}(p, \alpha)/(p, \gamma)$  branching ratio and the role of the NiCu cycle in shaping the final composition.

Another isotope,  $^{64}\text{Zn}$ , also exhibits a bimodal distribution, but its behavior differs from that of  $^{55}\text{Co}$ , as shown in Figures 8 and 9. In this case, the bimodal distribution is primarily caused by the single reaction  $^{65}\text{As}(p, \gamma)^{66}\text{Se}$  ( $r_s = -0.79$ ).  $^{59}\text{Cu}(p, \alpha)^{56}\text{Ni}$  ( $r_s = 0.15$ ) and  $^{59}\text{Cu}(p, \gamma)^{60}\text{Zn}$  ( $r_s = -0.15$ ) also show weak correlations with  $^{64}\text{Zn}$ , leading to a sparse cluster in the region of the back ellipse as shown in Figure 8. An additional 100,000 Monte Carlo trials were performed, varying only  $^{65}\text{As}(p, \gamma)^{66}\text{Se}$ , and the results are consistent.

The reaction paths reveal the origin of the bimodal distribution. Figure 10 shows the diagrams of integrated net fluxes for two representative Monte Carlo trials at

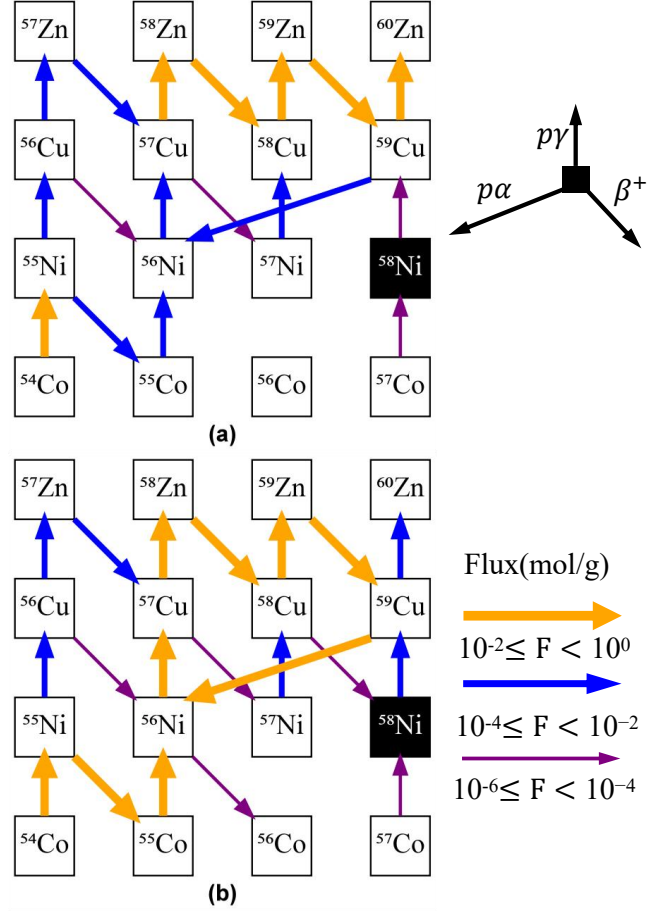


**Figure 7.** Diagrams of integrated net fluxes for Model K04 at the end of the trajectory. (a) Standard rates. (b) A representative Monte Carlo trial for  $\sigma = 2.3$  in which the randomly sampled ratio,  $^{59}\text{Cu}(p, \alpha)^{56}\text{Ni} / ^{59}\text{Cu}(p, \gamma)^{60}\text{Zn}$ , exceeds 100, illustrating a strong preference for the  $(p, \alpha)$  channel. The stable nuclide  $^{58}\text{Ni}$  is shown as black-filled square. Flux strengths are indicated by arrow colors, with the corresponding color scale on the right.

the end of the trajectory. The reaction flux inevitably passes through the  $^{64}\text{Ge}$  ( $t_{1/2} \approx 63.7$  s) waiting point (Y. H. Lam et al. 2022c; X. Zhou et al. 2023). In Figure 10(a), the first peak of  $^{64}\text{Zn}$  abundance is associated with higher  $^{65}\text{As}(p, \gamma)^{66}\text{Se}$  rates. The reaction flow mainly breaks out of the ZnGa cycle through the  $^{63}\text{Ga}(p, \gamma)^{64}\text{Ge}(p, \gamma)^{65}\text{As}$  path. This transfers more material through the region above Se, as reported by Y. H. Lam et al. (2022b, 2025), and results in lower abundances of  $^{64}\text{Ge}$  and  $^{64}\text{Ga}$ . In Figure 10(b), the second peak of  $^{64}\text{Zn}$  abundance is associated with lower  $^{65}\text{As}(p, \gamma)^{66}\text{Se}$  rates. The breakout occurs primarily via the alternative  $^{64}\text{Ga}(p, \gamma)^{65}\text{Ge}(p, \gamma)^{66}\text{As}$  path, which leaves more material of  $^{64}\text{Ge}$  and  $^{64}\text{Ga}$ . As a result, the decay of  $^{64}\text{Ge}$  and  $^{64}\text{Ga}$  finally leads to a bimodal abundance distribution of  $^{64}\text{Zn}$ .



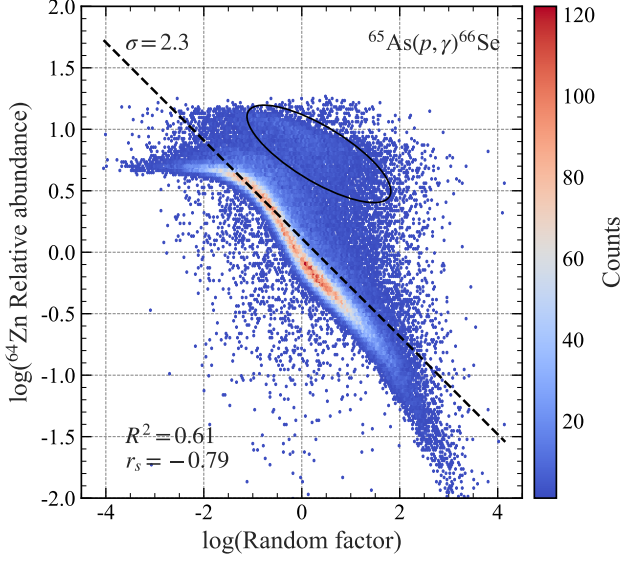


**Figure 8.** Similar to Figure 3, but showing a good correlation between  $^{65}\text{As}(p, \gamma)^{66}\text{Se}$  and  $^{64}\text{Zn}$  for  $\sigma = 2.3$  in Model K04.  $^{59}\text{Cu}(p, \alpha)^{56}\text{Ni}$  ( $r_s = 0.15$ ) and  $^{59}\text{Cu}(p, \gamma)^{60}\text{Zn}$  ( $r_s = -0.15$ ) show weak correlations with  $^{64}\text{Zn}$ , leading to a sparse cluster in the region of the black ellipse.

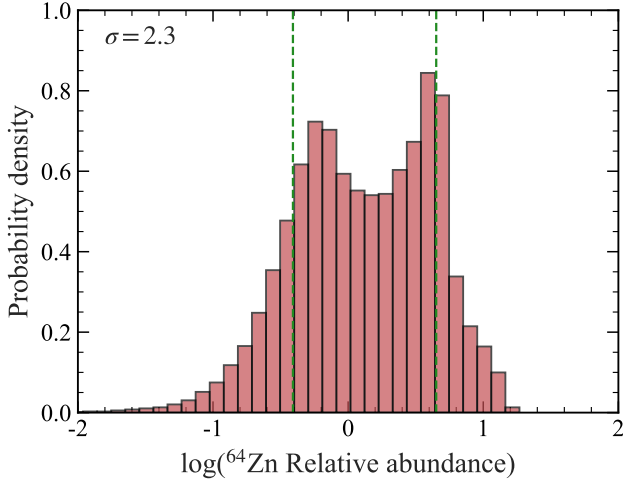


**Figure 9.** Similar to Figure 4, but showing the distribution of the  $^{64}\text{Zn}$  abundance for  $\sigma = 2.3$  in Model K04. The green dashed lines mark the 68% C.I.

Figure 11 compares the impact of  $\sigma = 1.15$  and  $\sigma = 2.3$  on the final abundances of Models K04, S01, and S16. The relative abundances and uncertainties are shown as a function of mass number. Here, the relative abundances correspond to the median values (50<sup>th</sup> percentile) from the Monte Carlo trials, normalized to the baseline abundances and restricted to mass numbers for which  $X_{\text{base}} \geq 10^{-6}$ . Based on nominal coverage probabilities with a factor of 10 applied to the reaction rates,

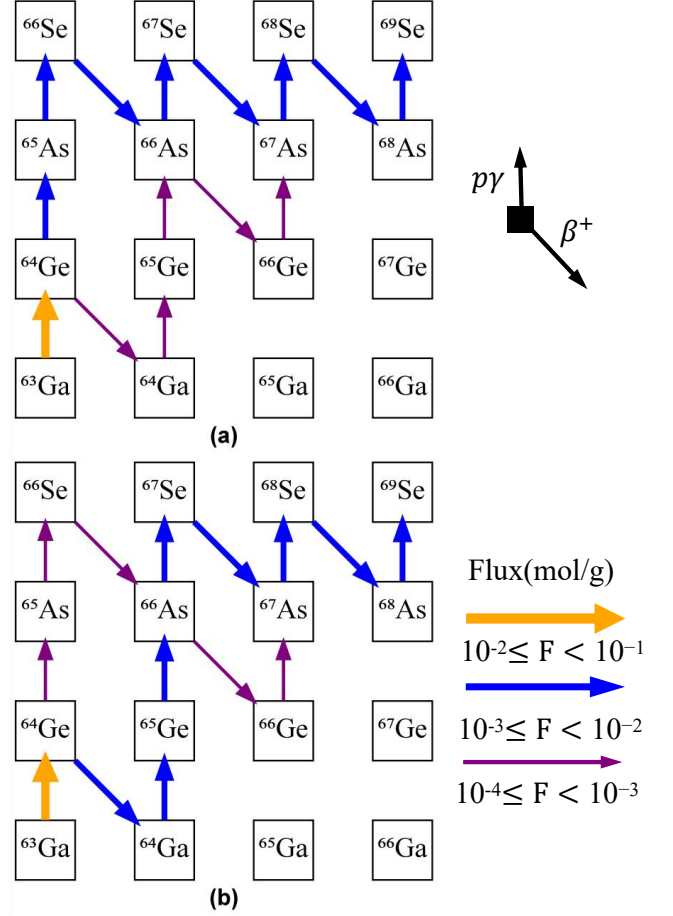


**Figure 10.** Diagrams of integrated net fluxes for  $\sigma = 2.3$  in Model K04 at the end of the trajectory. (a) A representative Monte Carlo trial corresponding to the peak at low  $^{64}\text{Zn}$  abundance. (b) A representative Monte Carlo trial corresponding to the peak at high  $^{64}\text{Zn}$  abundance. The two trials follow different dominant reaction paths, as indicated by the blue arrows.  $^{64}\text{Zn}$  is the waiting point in the network. Flux strengths are indicated by arrow colors, with the corresponding color scale on the right.

the uncertainties are estimated as 95% C.I. for  $\sigma = 1.15$  and 68% C.I. for  $\sigma = 2.3$ .

The uncertainties for  $\sigma = 2.3$  are generally larger than those for  $\sigma = 1.15$ . In particular, for Model S01, as shown in Figure 11(b), the uncertainties for mass number  $A = 1, 14, 15, 18, 21, 23$  (corresponding to isotopes  $^1\text{H}$ ,  $^{14}\text{N}$ ,  $^{15}\text{N}$ ,  $^{18}\text{F}$ ,  $^{21}\text{Ne}$ , and  $^{23}\text{Na}$ ) are noticeably overestimated, exceeding a factor of 10,000. The relative abundances are more stable for  $\sigma = 1.15$  compared to  $\sigma = 2.3$ . For Models K04 and S01, with mass number  $A > 80$ , the relative abundances exhibit a clear decreasing trend for  $\sigma = 2.3$  compared to  $\sigma = 1.15$ , as shown in Figure 11(a,c). At the mass number  $A = 50-80$ . Some mass numbers with small uncertainties reveal the existence of the waiting-point nuclides  $^{68}\text{Se}$ ,  $^{72}\text{Kr}$ ,  $^{76}\text{Sr}$  (L.

van Wormer et al. 1994; S. E. Woosley et al. 2004; H. Schatz 2006), and  $^{80}\text{Zr}$  (A. Parikh et al. 2013). Moreover,  $^{64}\text{Ge}$  (S. E. Woosley et al. 2004; H. Schatz 2006; X. Zhou et al. 2023) is identified as an additional waiting-point nuclide in Models S01 and S16.

### 3.2. Temperature-dependent Monte Carlo Simulations

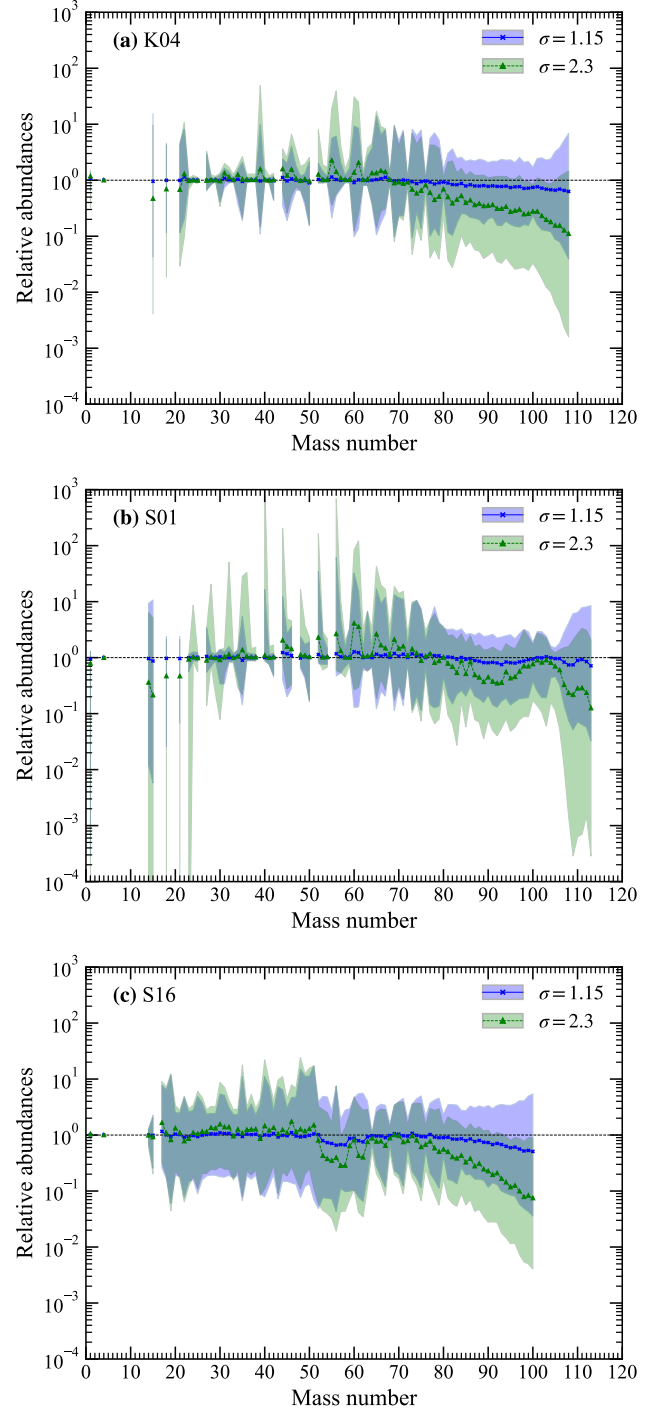
Figure 12 illustrates the effect of variations in the  $^{69}\text{Se}(p,\gamma)^{70}\text{Br}$  reaction rate on the abundance of  $^{69}\text{Ge}$  in Model K04. The Spearman correlation coefficient,  $r_s = -0.98$ , is consistent with the value of  $r_s = -0.97$  obtained for  $\sigma = 1.15$ . The abundance uncertainty from the temperature-dependent Monte Carlo simulations is 95.6 (68% C.I.), comparable to the 94.2 (95% C.I.) obtained from the temperature-independent simulations at  $\sigma = 1.15$  (see also Table 2). However, the distribution shape resembles that for  $\sigma = 2.3$  in Figure 3(b). Isotopes  $^{55}\text{Co}$  and  $^{64}\text{Zn}$  similarly exhibit a bimodal distribution, due to the same mechanisms as those described above for  $\sigma = 2.3$ .

Figure 13 compares results obtained from the temperature-dependent Monte Carlo simulations using STARLIB with those from previous temperature-independent Monte Carlo simulations. For the temperature-dependent Monte Carlo simulations, the relative abundances are determined following the same procedure as for the temperature-independent simulations: the relative abundances correspond to the median values from the Monte Carlo trials, normalized to the baseline abundances, and restricted to mass numbers for which  $X_{\text{base}} \geq 10^{-6}$ . Based on the nominal coverage probability of 68% for *f.u.* provided by STARLIB, the abundance uncertainties are estimated as 68% C.I. For Model S01, the baseline abundances with  $X_{\text{med}} \geq 10^{-6}$  extend up to  $A = 118$ , whereas they reach only  $A = 112$  in the temperature-independent Monte Carlo simulations. For Model K04, both approaches produce the same upper mass number. For Model S16, the corresponding limits are  $A = 96$  and  $A = 97$ , respectively. This reveals differences between the median (recommended) rates from STARLIB and REACLIB from high to low peak temperatures in XRB nucleosynthesis.

The abundance uncertainties are generally lower in the temperature-dependent Monte Carlo simulations compared with the temperature-independent simulations. For Model S01, the uncertainties significantly decrease when using STARLIB compared to adopting  $\sigma = 2.3$  (Figure 13(d)). For Models S01 and S16, the relative abundances also exhibit a clear decreasing trend for mass numbers  $A > 80$ , similar to the case with  $\sigma = 2.3$ . In particular, for Model S16, the relative abundances closely match those obtained with  $\sigma = 2.3$ .

### 3.3. Summary of Key Reactions

We present the recommended key reactions identified from the temperature-dependent Monte Carlo simulations using STARLIB and from the temperature-



**Figure 11.** The relative abundances obtained from the temperature-independent Monte Carlo simulations for Models K04, S01, and S16 (top to bottom). Blue shade indicates a 95% C.I. for  $\sigma = 1.15$ , and green shade corresponds to a 68% C.I. for  $\sigma = 2.3$ . The relative abundances for  $X_{\text{base}} \leq 10^{-6}$  don't plotted.

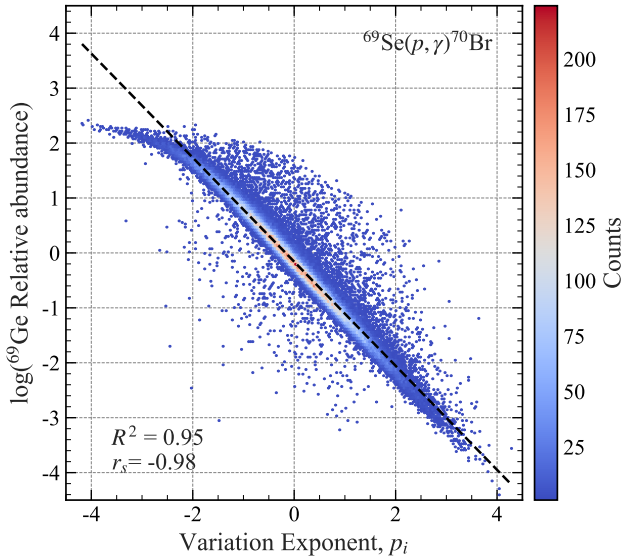


**Figure 12.** Similar to Figure 3, but showing a strong correlation between  $^{69}\text{Se}(p, \gamma)^{70}\text{Br}$  and  $^{69}\text{Ge}$  in the temperature-dependent Monte Carlo simulations for Model K04.

independent Monte Carlo simulations ( $\sigma = 1.15$  and  $\sigma = 2.3$ ) adopting REACLIB, as listed in Table 1. These key reactions were selected based on  $|r_s| \geq 0.50$ , considering isotopes with the baseline abundances  $X_{\text{base}} \geq 10^{-6}$  and the abundance uncertainties greater than or equal to a factor of two. The corresponding uncertainties are listed in Table 2.

#### 4. DISCUSSION AND CONCLUSION

We systematically investigate the impact of nuclear reaction rate uncertainties on XRB nucleosynthesis using both temperature-independent and -dependent methods. The simulations were performed for three representative XRB trajectories (Models K04, S01, and S16) using the WinNet code, with additional cross-checks done using the NucNet Tools (B. S. Meyer et al. 2007) and the SkyNet code (J. Lippuner & L. F. Roberts 2017). Although slight differences exist in the final abundances calculated by these codes, the overall results are in good agreement. Our approach included 100,000 Monte Carlo trials per model run, enabling a comprehensive exploration of how final isotopic abundances are affected by variations across a large number of reactions.

Results from temperature-independent Monte Carlo simulations indicate that the choice of lognormal parameters significantly affects isotope uncertainties. For modest perturbations ( $\sigma = 1.15$ ), isotopic abundances exhibit limited variability, and the effect of individual reactions is more pronounced, typically producing high Spearman correlation coefficients. In contrast, with larger perturbations ( $\sigma = 2.3$ ), uncertainties increase substantially, and the coupling among multiple competing reactions becomes more prominent. This reduces the linear correlation between individual reaction rates and

final abundances, resulting in lower Spearman correlation coefficients.

Large perturbations also lead to greater variability and, in some cases, multi-peaked abundance distributions. These multi-peak structures can arise not only from coupled reaction effects but also, in certain cases, from a single reaction, exemplified by  $^{55}\text{Co}$  and  $^{64}\text{Zn}$ . Conversely, smaller perturbations lead to less variability and predominantly single-peaked distributions, consistent with earlier studies (A. Parikh et al. 2008; F. Moreno & J. José 2009).

Temperature-dependent Monte Carlo simulations using STARLIB further incorporate more realistic, temperature-dependent rate uncertainties. We recommend using the temperature-dependent Monte Carlo method with STARLIB as the primary approach, while the temperature-independent Monte Carlo method with modest perturbations (e.g.,  $\sigma = 1.15$ ) can be used for supplementary analysis. Across all models, the key reactions identified largely align with previous studies (A. Parikh et al. 2008; F. Moreno & J. José 2009; R. H. Cyburt et al. 2016). These findings offer insights for future experimental and theoretical efforts to reduce reaction rate uncertainties. In particular, reactions that show consistent strong correlations across multiple models and simulation methods should be prioritized for improved measurements.

When using the temperature-independent Monte Carlo method, the lognormal parameter  $\sigma$  should be carefully chosen, and reaction uncertainties should be considered in terms of their coverage probabilities; each reaction should have its own uncertainty limit rather than applying the same uncertainty to all reactions. The temperature-dependent Monte Carlo method using STARLIB provides a more reliable, physically motivated assessment of abundance uncertainties than the temperature-independent method. Multi-peaked abundance distributions naturally emerge from competing reaction pathways under large perturbations, emphasising the non-linear, non-monotonic nature of XRB nucleosynthesis and warranting further study.

Overall, this work advances our understanding of XRB nucleosynthesis and highlights the importance of incorporating realistic, temperature-dependent reaction rate uncertainties. Future studies could extend this approach to 1D multizone hydrodynamic models, thereby providing an even more comprehensive assessment of reaction rate uncertainties in XRB nucleosynthesis.

#### ACKNOWLEDGMENTS

The authors thank the reviewer for her/his valuable comments on the submitted manuscript. We thank H. Schatz for providing XRB trajectories used in this study. We acknowledge support from the National Natural Science Foundation of China (No. 12175152), LingChuang

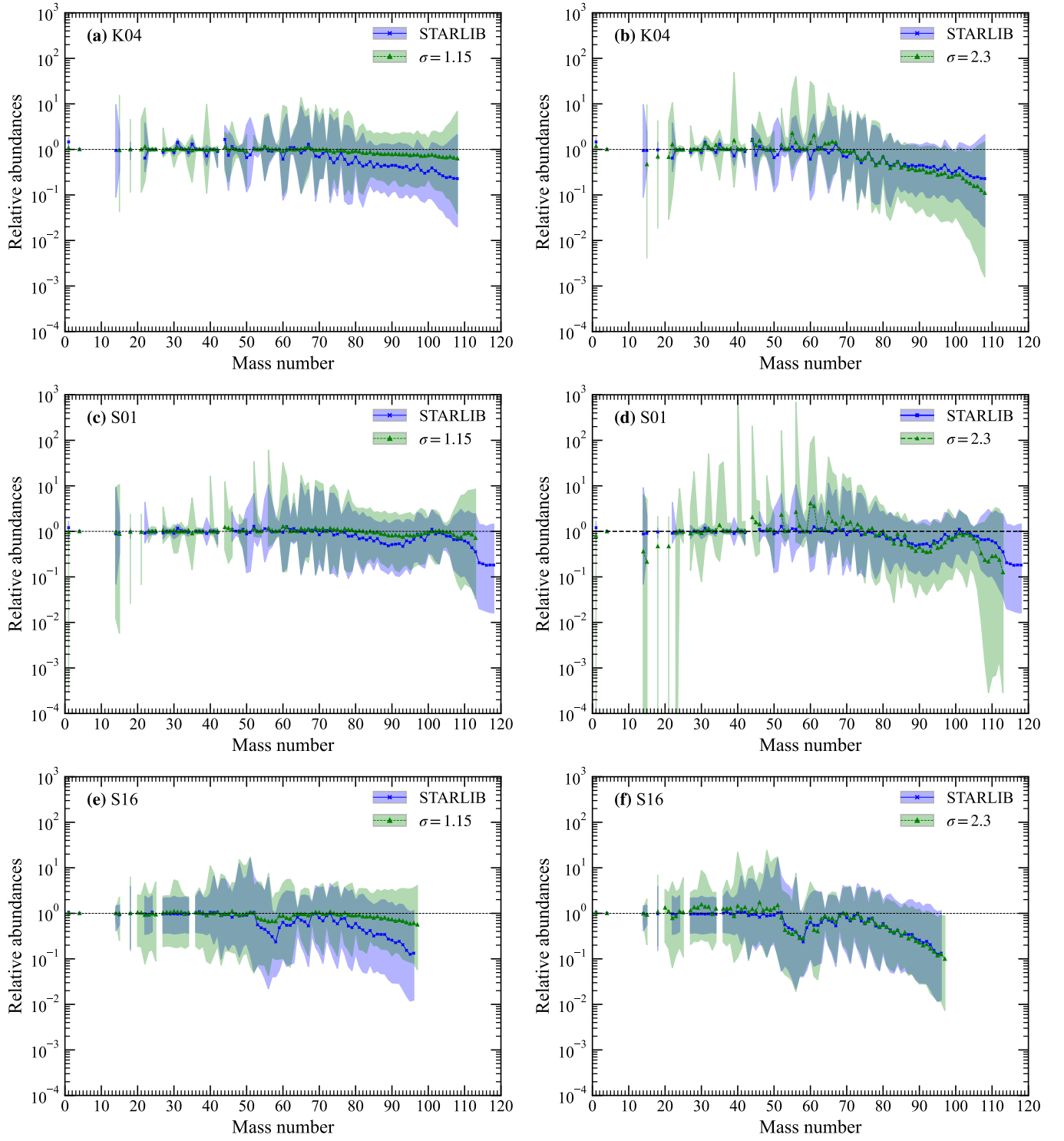


**Figure 13.** Similar to Figure 11, but comparing results from the temperature-dependent Monte Carlo simulations (STARLIB) with those from the temperature-independent simulations  $\sigma = 1.15$  (left panels) and  $\sigma = 2.3$  (right panels) for Models K04, S01, and S16 (top to bottom). The abundance uncertainties are estimated as 68% C.I. in temperature-dependent Monte Carlo simulations due to the nominal coverage probability of 68% for *f.u.* provided by STARLIB.



Research Project of China National Nuclear Corporation (Nos. 2025-084, 2024-065, 2024-068).

*Software:* IPython (F. Pérez & B. E. Granger 2007), Jupyter (T. Kluyver et al. 2016), matplotlib (J. D. Hunter 2007), numpy (C. R. Harris et al. 2020), scipy (P.

Virtanen et al. 2020), scikit-learn (F. Pedregosa et al. 2011), seaborn (M. L. Waskom 2021), NucNet Tools (B. S. Meyer et al. 2007), SkyNet (J. Lippuner & L. F. Roberts 2017), WinNet (C. Winteler et al. 2012; M. Reichert et al. 2023)

## APPENDIX

**Table 1.** The Spearman correlation coefficients  $r_s$  between reactions and isotopes of Models K04, S01, and S16 for the temperature-dependent (STARLIB) and -independent Monte Carlo simulations ( $\sigma = 1.15$  and  $\sigma = 2.3$ ). Only  $|r_s| \geq 0.50$  with isotopic baseline abundances  $X_{\text{base}} \geq 10^{-6}$  and uncertainties equal to or exceeding a factor of 2 are listed.

| Reaction                                      | Isotope          | Model K04 |                 |                | Model S01 |                 |                | Model S16 |                 |                |
|---|------------------|-----------|-----------------|----------------|-----------|-----------------|----------------|-----------|-----------------|----------------|
|   |                  | STARLIB   | $\sigma = 1.15$ | $\sigma = 2.3$ | STARLIB   | $\sigma = 1.15$ | $\sigma = 2.3$ | STARLIB   | $\sigma = 1.15$ | $\sigma = 2.3$ |
| $^{14}\text{O}(\alpha, p)^{17}\text{F}$       | $^{14}\text{N}$  | −0.97     | ...             | ...            | −0.92     | −0.95           | −0.57          | −0.98     | ...             | −0.85          |
|   | $^{15}\text{N}$  | ...       | ...             | ...            | ...       | ...             | ...            | 0.76      | ...             | ...            |
|   | $^{18}\text{F}$  | ...       | ...             | ...            | ...       | ...             | ...            | 0.99      | 1.00            | 0.88           |
| $^{15}\text{O}(\alpha, \gamma)^{19}\text{Ne}$ | $^{15}\text{N}$  | −0.85     | −0.75           | −0.60          | −0.88     | −0.80           | ...            | −0.56     | −0.94           | −0.82          |
|   | $^{20}\text{Ne}$ | ...       | ...             | ...            | ...       | ...             | ...            | ...       | 0.96            | 0.85           |
|   | $^{21}\text{Ne}$ | ...       | ...             | ...            | ...       | ...             | ...            | ...       | 0.97            | 0.89           |
|   | $^{22}\text{Na}$ | ...       | ...             | ...            | ...       | ...             | ...            | 0.81      | 0.57            | 0.54           |
|   | $^{23}\text{Na}$ | ...       | ...             | ...            | ...       | ...             | ...            | 0.88      | 0.83            | 0.73           |
|   | $^{24}\text{Mg}$ | ...       | ...             | ...            | ...       | ...             | ...            | 0.86      | 0.85            | 0.77           |
|   | $^{25}\text{Mg}$ | ...       | ...             | ...            | ...       | ...             | ...            | ...       | 0.58            | 0.58           |
|   | $^{27}\text{Al}$ | ...       | ...             | ...            | ...       | ...             | ...            | 0.89      | 0.95            | 0.85           |
|   | $^{28}\text{Si}$ | ...       | ...             | ...            | ...       | ...             | ...            | 0.89      | 0.95            | 0.85           |
|   | $^{29}\text{Si}$ | ...       | ...             | ...            | ...       | ...             | ...            | 0.89      | 0.95            | 0.84           |
|   | $^{30}\text{Si}$ | ...       | ...             | ...            | ...       | ...             | ...            | 0.83      | 0.74            | 0.64           |
|   | $^{31}\text{P}$  | ...       | ...             | ...            | ...       | ...             | ...            | 0.87      | 0.74            | 0.66           |
|   | $^{32}\text{S}$  | ...       | ...             | ...            | ...       | ...             | ...            | 0.88      | 0.86            | 0.75           |
|   | $^{33}\text{S}$  | ...       | ...             | ...            | ...       | ...             | ...            | 0.87      | 0.91            | 0.74           |
|   | $^{34}\text{S}$  | ...       | ...             | ...            | ...       | ...             | ...            | 0.88      | 0.94            | 0.84           |
|   | $^{36}\text{Ar}$ | ...       | ...             | ...            | ...       | ...             | ...            | 0.86      | 0.89            | 0.80           |
|   | $^{37}\text{Ar}$ | ...       | ...             | ...            | ...       | ...             | ...            | 0.71      | 0.76            | 0.63           |
|   | $^{38}\text{Ar}$ | ...       | ...             | ...            | ...       | ...             | ...            | 0.85      | 0.94            | 0.82           |
|   | $^{39}\text{K}$  | ...       | ...             | ...            | ...       | ...             | ...            | 0.84      | 0.61            | 0.55           |
|   | $^{40}\text{Ca}$ | ...       | ...             | ...            | ...       | ...             | ...            | 0.78      | ...             | ...            |
|   | $^{41}\text{Ca}$ | ...       | ...             | ...            | ...       | ...             | ...            | ...       | 0.53            | ...            |
|   | $^{42}\text{Ca}$ | ...       | ...             | ...            | ...       | ...             | ...            | 0.70      | 0.85            | 0.66           |

Table 1 *continued*

**Table 1** (*continued*)

| Reaction                                  | Isotope          | Model K04 |                 |                | Model S01 |                 |                | Model S16 |                 |                |
|---|------------------|-----------|-----------------|----------------|-----------|-----------------|----------------|-----------|-----------------|----------------|
|   |                  | STARLIB   | $\sigma = 1.15$ | $\sigma = 2.3$ | STARLIB   | $\sigma = 1.15$ | $\sigma = 2.3$ | STARLIB   | $\sigma = 1.15$ | $\sigma = 2.3$ |
| $^{18}\text{Ne}(\alpha, p)^{21}\text{Na}$ | $^{44}\text{Ti}$ | ...       | ...             | ...            | ...       | ...             | ...            | ...       | 0.60            | ...            |
|   | $^{45}\text{Ti}$ | ...       | ...             | ...            | ...       | ...             | ...            | ...       | 0.73            | 0.53           |
|   | $^{46}\text{Ti}$ | ...       | ...             | ...            | ...       | ...             | ...            | 0.59      | 0.59            | ...            |
|   | $^{47}\text{Ti}$ | ...       | ...             | ...            | ...       | ...             | ...            | ...       | 0.62            | ...            |
|   | $^{15}\text{N}$  | ...       | -0.62           | ...            | ...       | ...             | ...            | ...       | ...             | ...            |
|   | $^{18}\text{F}$  | -0.96     | -0.99           | -0.76          | ...       | -0.95           | -0.56          | ...       | ...             | ...            |
|   | $^{21}\text{Ne}$ | ...       | -0.99           | -0.77          | ...       | -0.95           | -0.57          | ...       | ...             | ...            |
| $^{22}\text{Mg}(p, \gamma)^{23}\text{Al}$ | $^{22}\text{Na}$ | ...       | ...             | ...            | ...       | ...             | ...            | ...       | -0.76           | -0.66          |
| $^{23}\text{Al}(p, \gamma)^{24}\text{Si}$ | $^{22}\text{Na}$ | -0.87     | -0.74           | ...            | -0.70     | ...             | ...            | ...       | ...             | ...            |
| $^{26}\text{P}(p, \gamma)^{27}\text{S}$   | $^{25}\text{Mg}$ | ...       | ...             | ...            | ...       | ...             | ...            | ...       | -0.74           | -0.57          |
| $^{27}\text{P}(p, \gamma)^{28}\text{S}$   | $^{27}\text{Al}$ | ...       | -0.96           | -0.73          | ...       | -0.90           | -0.55          | ...       | ...             | ...            |
| $^{30}\text{S}(p, \gamma)^{31}\text{Cl}$  | $^{30}\text{Si}$ | ...       | ...             | ...            | ...       | ...             | ...            | ...       | -0.54           | ...            |
| $^{31}\text{S}(p, \gamma)^{32}\text{Cl}$  | $^{31}\text{P}$  | ...       | ...             | ...            | ...       | ...             | ...            | ...       | -0.57           | -0.51          |
| $^{31}\text{Cl}(p, \gamma)^{32}\text{Ar}$ | $^{30}\text{Si}$ | ...       | -0.85           | -0.62          | ...       | -0.66           | ...            | ...       | ...             | ...            |
|   | $^{31}\text{P}$  | ...       | 0.65            | ...            | ...       | ...             | ...            | ...       | ...             | ...            |
| $^{34}\text{Ar}(p, \gamma)^{35}\text{K}$  | $^{34}\text{S}$  | ...       | -0.85           | -0.55          | ...       | -0.81           | ...            | ...       | ...             | ...            |
|   | $^{35}\text{Cl}$ | ...       | 0.87            | 0.58           | ...       | 0.85            | ...            | ...       | ...             | ...            |
| $^{39}\text{Ca}(p, \gamma)^{40}\text{Sc}$ | $^{39}\text{K}$  | -0.68     | -0.97           | -0.71          | -0.51     | ...             | ...            | ...       | -0.71           | -0.61          |
| $^{40}\text{Ca}(p, \gamma)^{41}\text{Sc}$ | $^{40}\text{Ca}$ | ...       | ...             | ...            | ...       | ...             | ...            | ...       | -0.83           | -0.79          |
| $^{41}\text{Sc}(p, \gamma)^{42}\text{Ti}$ | $^{41}\text{Ca}$ | ...       | ...             | ...            | ...       | ...             | ...            | -0.81     | -0.76           | -0.71          |
| $^{43}\text{Ti}(p, \gamma)^{44}\text{V}$  | $^{43}\text{Sc}$ | ...       | ...             | ...            | ...       | ...             | ...            | -0.83     | -0.83           | -0.73          |
| $^{44}\text{Ti}(p, \gamma)^{45}\text{V}$  | $^{44}\text{Ti}$ | ...       | ...             | ...            | ...       | ...             | ...            | -0.72     | -0.62           | -0.61          |
| $^{43}\text{V}(p, \gamma)^{44}\text{Cr}$  | $^{42}\text{Ca}$ | -0.86     | -0.88           | -0.61          | -0.67     | -0.71           | ...            | ...       | ...             | ...            |
|   | $^{44}\text{Ti}$ | 0.76      | 0.68            | 0.53           | ...       | 0.55            | ...            | ...       | ...             | ...            |
| $^{45}\text{V}(p, \gamma)^{46}\text{Cr}$  | $^{45}\text{Ti}$ | ...       | ...             | ...            | ...       | ...             | ...            | -0.76     | ...             | ...            |
|   | $^{46}\text{Ti}$ | ...       | ...             | ...            | ...       | ...             | ...            | ...       | 0.53            | ...            |
| $^{47}\text{V}(p, \gamma)^{48}\text{Cr}$  | $^{47}\text{Ti}$ | ...       | ...             | ...            | ...       | ...             | ...            | -0.58     | ...             | -0.51          |
| $^{46}\text{Cr}(p, \gamma)^{47}\text{Mn}$ | $^{46}\text{Ti}$ | -0.51     | -0.90           | -0.63          | -0.60     | -0.89           | -0.54          | ...       | ...             | ...            |
|   | $^{48}\text{Cr}$ | ...       | ...             | ...            | ...       | 0.53            | ...            | ...       | ...             | ...            |
| $^{48}\text{Cr}(p, \gamma)^{49}\text{Mn}$ | $^{48}\text{Cr}$ | ...       | ...             | ...            | ...       | ...             | ...            | -0.90     | -0.86           | -0.85          |
| $^{49}\text{Cr}(p, \gamma)^{50}\text{Mn}$ | $^{49}\text{V}$  | ...       | ...             | ...            | ...       | ...             | ...            | -0.66     | -0.78           | -0.73          |
| $^{50}\text{Cr}(p, \gamma)^{51}\text{Mn}$ | $^{50}\text{Cr}$ | ...       | ...             | ...            | ...       | ...             | ...            | -0.71     | -0.78           | -0.73          |
| $^{46}\text{Mn}(p, \gamma)^{47}\text{Fe}$ | $^{44}\text{Ti}$ | ...       | -0.64           | ...            | ...       | -0.61           | ...            | ...       | ...             | ...            |
|   | $^{45}\text{Ti}$ | -0.86     | -0.91           | -0.64          | ...       | -0.77           | ...            | ...       | ...             | ...            |
|   | $^{46}\text{Ti}$ | 0.51      | ...             | ...            | ...       | ...             | ...            | ...       | ...             | ...            |
| $^{47}\text{Mn}(p, \gamma)^{48}\text{Fe}$ | $^{47}\text{Ti}$ | ...       | -0.69           | ...            | ...       | ...             | ...            | ...       | ...             | ...            |
| $^{51}\text{Mn}(p, \gamma)^{52}\text{Fe}$ | $^{51}\text{Cr}$ | ...       | ...             | ...            | ...       | ...             | ...            | -0.92     | -0.91           | -0.89          |

**Table 1** *continued*

**Table 1** (*continued*)

| Reaction                                  | Isotope          | Model K04 |                 |                | Model S01 |                 |                | Model S16 |                 |                |
|---|------------------|-----------|-----------------|----------------|-----------|-----------------|----------------|-----------|-----------------|----------------|
|   |                  | STARLIB   | $\sigma = 1.15$ | $\sigma = 2.3$ | STARLIB   | $\sigma = 1.15$ | $\sigma = 2.3$ | STARLIB   | $\sigma = 1.15$ | $\sigma = 2.3$ |
| $^{52}\text{Mn}(p, \gamma)^{53}\text{Fe}$ | $^{52}\text{Mn}$ | ...       | ...             | ...            | ...       | ...             | ...            | ...       | -0.71           | -0.69          |
| $^{50}\text{Fe}(p, \gamma)^{51}\text{Co}$ | $^{50}\text{Cr}$ | -0.93     | -0.90           | -0.68          | -0.85     | -0.81           | -0.50          | ...       | ...             | ...            |
| $^{51}\text{Fe}(p, \gamma)^{52}\text{Co}$ | $^{51}\text{Cr}$ | -0.95     | ...             | ...            | -0.89     | ...             | ...            | ...       | ...             | ...            |
| $^{52}\text{Fe}(p, \gamma)^{53}\text{Co}$ | $^{52}\text{Fe}$ | -0.68     | -0.64           | ...            | -0.71     | -0.60           | ...            | -0.97     | -0.97           | -0.92          |
| $^{53}\text{Fe}(p, \gamma)^{54}\text{Co}$ | $^{53}\text{Mn}$ | ...       | ...             | ...            | ...       | ...             | ...            | -0.89     | -0.93           | -0.85          |
| $^{54}\text{Fe}(p, \gamma)^{55}\text{Co}$ | $^{54}\text{Fe}$ | ...       | ...             | ...            | ...       | ...             | ...            | -0.90     | -0.92           | -0.85          |
| $^{50}\text{Co}(p, \gamma)^{51}\text{Ni}$ | $^{49}\text{V}$  | -0.74     | -0.88           | -0.57          | -0.55     | -0.69           | ...            | ...       | ...             | ...            |
| $^{52}\text{Co}(p, \gamma)^{53}\text{Ni}$ | $^{52}\text{Fe}$ | ...       | -0.55           | ...            | ...       | -0.51           | ...            | ...       | ...             | ...            |
| $^{53}\text{Co}(p, \gamma)^{54}\text{Ni}$ | $^{53}\text{Mn}$ | ...       | ...             | -0.60          | -0.56     | -0.79           | -0.54          | ...       | ...             | ...            |
| $^{55}\text{Co}(p, \gamma)^{56}\text{Ni}$ | $^{55}\text{Co}$ | ...       | ...             | ...            | ...       | ...             | ...            | -0.91     | -0.87           | -0.84          |
| $^{55}\text{Ni}(p, \gamma)^{56}\text{Cu}$ | $^{55}\text{Co}$ | -0.80     | ...             | ...            | -0.81     | ...             | ...            | ...       | ...             | ...            |
| $^{56}\text{Ni}(p, \gamma)^{57}\text{Cu}$ | $^{56}\text{Ni}$ | -0.90     | -0.92           | -0.67          | -0.84     | -0.84           | -0.50          | -0.94     | -0.91           | -0.85          |
| $^{57}\text{Ni}(p, \gamma)^{58}\text{Cu}$ | $^{57}\text{Ni}$ | ...       | ...             | ...            | ...       | ...             | ...            | -0.82     | -0.69           | -0.70          |
|   | $^{58}\text{Ni}$ | ...       | ...             | ...            | ...       | ...             | ...            | ...       | 0.55            | ...            |
| $^{58}\text{Ni}(p, \gamma)^{59}\text{Cu}$ | $^{58}\text{Ni}$ | ...       | ...             | ...            | ...       | ...             | ...            | -0.55     | ...             | ...            |
| $^{56}\text{Cu}(p, \gamma)^{57}\text{Zn}$ | $^{55}\text{Co}$ | ...       | -0.72           | ...            | ...       | ...             | ...            | ...       | ...             | ...            |
| $^{57}\text{Cu}(p, \gamma)^{58}\text{Zn}$ | $^{57}\text{Ni}$ | -0.78     | -0.76           | -0.55          | -0.80     | -0.78           | ...            | ...       | ...             | ...            |
| $^{58}\text{Cu}(p, \gamma)^{59}\text{Zn}$ | $^{58}\text{Ni}$ | ...       | ...             | ...            | -0.72     | -0.56           | ...            | ...       | ...             | -0.57          |
| $^{59}\text{Cu}(p, \gamma)^{60}\text{Zn}$ | $^{59}\text{Ni}$ | ...       | ...             | -0.66          | ...       | -0.79           | -0.53          | -0.82     | -0.84           | -0.87          |
| $^{60}\text{Zn}(p, \gamma)^{61}\text{Ga}$ | $^{60}\text{Ni}$ | ...       | ...             | ...            | ...       | ...             | ...            | -0.59     | -0.66           | -0.62          |
| $^{61}\text{Zn}(p, \gamma)^{62}\text{Ga}$ | $^{61}\text{Cu}$ | ...       | ...             | ...            | ...       | ...             | ...            | ...       | -0.55           | -0.53          |
| $^{62}\text{Zn}(p, \gamma)^{63}\text{Ga}$ | $^{62}\text{Zn}$ | ...       | ...             | ...            | ...       | ...             | ...            | ...       | -0.55           | -0.55          |
| $^{65}\text{Zn}(p, \gamma)^{66}\text{Ga}$ | $^{66}\text{Ga}$ | ...       | ...             | ...            | ...       | ...             | ...            | ...       | 0.62            | 0.51           |
| $^{61}\text{Ga}(p, \gamma)^{62}\text{Ge}$ | $^{60}\text{Ni}$ | -0.92     | -0.93           | -0.69          | -0.78     | -0.81           | -0.50          | -0.70     | -0.65           | -0.57          |
|   | $^{61}\text{Ni}$ | ...       | ...             | ...            | ...       | ...             | ...            | -0.57     | ...             | ...            |
|   | $^{62}\text{Ni}$ | ...       | ...             | ...            | ...       | ...             | ...            | -0.56     | -0.61           | -0.56          |
|   | $^{61}\text{Cu}$ | -0.93     | -0.97           | -0.70          | -0.81     | -0.89           | -0.55          | -0.66     | -0.63           | -0.62          |
|   | $^{62}\text{Zn}$ | ...       | ...             | ...            | ...       | 0.54            | ...            | -0.54     | -0.56           | -0.52          |
|   | $^{64}\text{Zn}$ | ...       | ...             | ...            | ...       | ...             | ...            | 0.77      | ...             | ...            |
|   | $^{68}\text{Ge}$ | ...       | ...             | ...            | ...       | ...             | ...            | 0.76      | ...             | ...            |
|   | $^{72}\text{Se}$ | ...       | ...             | ...            | ...       | ...             | ...            | 0.72      | ...             | ...            |
|   | $^{76}\text{Kr}$ | ...       | ...             | ...            | ...       | ...             | ...            | 0.69      | ...             | ...            |
|   | $^{80}\text{Sr}$ | ...       | ...             | ...            | ...       | ...             | ...            | 0.64      | ...             | ...            |
|   | $^{84}\text{Sr}$ | ...       | ...             | ...            | ...       | ...             | ...            | 0.58      | ...             | ...            |
|   | $^{85}\text{Y}$  | ...       | ...             | ...            | ...       | ...             | ...            | 0.56      | ...             | ...            |
|   | $^{86}\text{Zr}$ | ...       | ...             | ...            | ...       | ...             | ...            | 0.58      | ...             | ...            |
|   | $^{87}\text{Zr}$ | ...       | ...             | ...            | ...       | ...             | ...            | 0.53      | ...             | ...            |

**Table 1** *continued*

Table 1 (continued)

| Reaction                                  | Isotope          | Model K04 |                 |                | Model S01 |                 |                | Model S16 |                 |                |
|---|------------------|-----------|-----------------|----------------|-----------|-----------------|----------------|-----------|-----------------|----------------|
|   |                  | STARLIB   | $\sigma = 1.15$ | $\sigma = 2.3$ | STARLIB   | $\sigma = 1.15$ | $\sigma = 2.3$ | STARLIB   | $\sigma = 1.15$ | $\sigma = 2.3$ |
|   | $^{88}\text{Zr}$ | ...       | ...             | ...            | ...       | ...             | ...            | 0.53      | ...             | ...            |
|   | $^{89}\text{Nb}$ | ...       | ...             | ...            | ...       | ...             | ...            | 0.53      | ...             | ...            |
|   | $^{91}\text{Nb}$ | ...       | ...             | ...            | ...       | ...             | ...            | 0.55      | ...             | ...            |
|   | $^{90}\text{Mo}$ | ...       | ...             | ...            | ...       | ...             | ...            | 0.51      | ...             | ...            |
|   | $^{92}\text{Mo}$ | ...       | ...             | ...            | ...       | ...             | ...            | 0.53      | ...             | ...            |
|   | $^{93}\text{Tc}$ | ...       | ...             | ...            | ...       | ...             | ...            | 0.51      | ...             | ...            |
|   | $^{94}\text{Tc}$ | ...       | ...             | ...            | ...       | ...             | ...            | 0.51      | ...             | ...            |
|   | $^{95}\text{Ru}$ | ...       | ...             | ...            | ...       | ...             | ...            | 0.50      | ...             | ...            |
|   | $^{96}\text{Ru}$ | ...       | ...             | ...            | ...       | ...             | ...            | 0.51      | ...             | ...            |
| $^{62}\text{Ga}(p, \gamma)^{63}\text{Ge}$ | $^{62}\text{Zn}$ | -0.70     | ...             | ...            | -0.68     | ...             | ...            | ...       | ...             | ...            |
| $^{63}\text{Ga}(p, \gamma)^{64}\text{Ge}$ | $^{63}\text{Cu}$ | -0.57     | -0.94           | -0.78          | -0.72     | -0.89           | -0.63          | -0.60     | -0.55           | -0.64          |
| $^{64}\text{Ga}(p, \gamma)^{65}\text{Ge}$ | $^{65}\text{Zn}$ | ...       | ...             | ...            | ...       | ...             | ...            | 0.80      | 0.92            | 0.77           |
|   | $^{66}\text{Ga}$ | ...       | ...             | ...            | ...       | ...             | ...            | ...       | 0.55            | ...            |
| $^{65}\text{Ge}(p, \gamma)^{66}\text{As}$ | $^{65}\text{Zn}$ | -0.83     | -0.86           | -0.78          | -0.89     | -0.89           | -0.65          | ...       | ...             | ...            |
|   | $^{66}\text{Ge}$ | ...       | ...             | ...            | ...       | ...             | ...            | ...       | 0.53            | ...            |
| $^{66}\text{Ge}(p, \gamma)^{67}\text{As}$ | $^{66}\text{Ge}$ | ...       | ...             | ...            | -0.64     | -0.65           | ...            | ...       | -0.55           | ...            |
| $^{65}\text{As}(p, \gamma)^{66}\text{Se}$ | $^1\text{H}$     | ...       | -0.55           | ...            | ...       | ...             | ...            | ...       | ...             | ...            |
|   | $^{64}\text{Zn}$ | -0.94     | -0.97           | -0.79          | -0.74     | -0.70           | -0.54          | ...       | ...             | ...            |
|   | $^{67}\text{Ga}$ | -0.57     | -0.63           | ...            | ...       | ...             | ...            | ...       | ...             | ...            |
|   | $^{66}\text{Ge}$ | ...       | -0.51           | ...            | ...       | ...             | ...            | ...       | ...             | ...            |
|   | $^{68}\text{Ge}$ | ...       | ...             | ...            | ...       | ...             | ...            | ...       | 0.75            | 0.56           |
|   | $^{72}\text{Se}$ | ...       | ...             | ...            | ...       | ...             | ...            | 0.53      | 0.78            | 0.58           |
|   | $^{76}\text{Kr}$ | ...       | ...             | ...            | ...       | ...             | ...            | 0.51      | 0.74            | 0.55           |
|   | $^{80}\text{Sr}$ | ...       | ...             | ...            | ...       | ...             | ...            | ...       | 0.66            | ...            |
| $^{66}\text{As}(p, \gamma)^{67}\text{Se}$ | $^{66}\text{Ge}$ | -0.70     | -0.71           | -0.55          | ...       | ...             | ...            | ...       | ...             | ...            |
| $^{67}\text{As}(p, \gamma)^{68}\text{Se}$ | $^{67}\text{Ga}$ | -0.59     | -0.63           | -0.66          | -0.86     | -0.89           | -0.68          | -0.74     | -0.80           | -0.80          |
| $^{68}\text{As}(p, \gamma)^{69}\text{Se}$ | $^{69}\text{Ge}$ | ...       | ...             | ...            | ...       | ...             | ...            | 0.66      | 0.81            | 0.65           |
| $^{69}\text{Se}(p, \gamma)^{70}\text{Br}$ | $^{69}\text{Ge}$ | -0.98     | -0.97           | -0.88          | -0.92     | -0.90           | -0.71          | ...       | ...             | ...            |
| $^{70}\text{Se}(p, \gamma)^{71}\text{Br}$ | $^{70}\text{Ge}$ | -0.73     | -0.66           | -0.57          | -0.86     | -0.84           | -0.64          | -0.58     | -0.68           | -0.57          |
| $^{70}\text{Br}(p, \gamma)^{71}\text{Kr}$ | $^{70}\text{Ge}$ | -0.53     | -0.63           | -0.51          | ...       | ...             | ...            | ...       | ...             | ...            |
| $^{71}\text{Br}(p, \gamma)^{72}\text{Kr}$ | $^{71}\text{As}$ | -0.93     | -0.95           | -0.80          | -0.92     | -0.91           | -0.70          | -0.78     | -0.86           | -0.81          |
| $^{72}\text{Br}(p, \gamma)^{73}\text{Kr}$ | $^{73}\text{Se}$ | ...       | ...             | ...            | ...       | ...             | ...            | 0.52      | 0.63            | 0.52           |
| $^{73}\text{Kr}(p, \gamma)^{74}\text{Rb}$ | $^{73}\text{Se}$ | -0.96     | -0.97           | -0.84          | -0.92     | -0.91           | -0.72          | -0.51     | -0.61           | -0.54          |
| $^{74}\text{Kr}(p, \gamma)^{75}\text{Rb}$ | $^{74}\text{Se}$ | -0.89     | -0.89           | -0.70          | -0.93     | -0.91           | -0.70          | -0.66     | -0.79           | -0.65          |
| $^{75}\text{Rb}(p, \gamma)^{76}\text{Sr}$ | $^{75}\text{Br}$ | -0.96     | -0.97           | -0.82          | -0.92     | -0.92           | -0.71          | -0.79     | -0.89           | -0.81          |
| $^{76}\text{Rb}(p, \gamma)^{77}\text{Sr}$ | $^{76}\text{Kr}$ | ...       | ...             | ...            | -0.66     | -0.57           | ...            | ...       | ...             | ...            |
| $^{77}\text{Sr}(p, \gamma)^{78}\text{Y}$  | $^{77}\text{Kr}$ | -0.93     | -0.97           | -0.79          | -0.81     | -0.90           | -0.67          | -0.57     | -0.72           | -0.58          |

Table 1 continued



Table 1 (continued)

| Reaction                                    | Isotope           | Model K04 |                 |                | Model S01 |                 |                | Model S16 |                 |                |
|---|-------------------|-----------|-----------------|----------------|-----------|-----------------|----------------|-----------|-----------------|----------------|
|   |                   | STARLIB   | $\sigma = 1.15$ | $\sigma = 2.3$ | STARLIB   | $\sigma = 1.15$ | $\sigma = 2.3$ | STARLIB   | $\sigma = 1.15$ | $\sigma = 2.3$ |
| $^{78}\text{Sr}(p, \gamma)^{79}\text{Y}$    | $^{78}\text{Kr}$  | -0.94     | -0.95           | -0.76          | -0.94     | -0.93           | -0.72          | -0.68     | -0.83           | -0.67          |
| $^{79}\text{Y}(p, \gamma)^{80}\text{Zr}$    | $^{79}\text{Kr}$  | -0.93     | -0.97           | -0.80          | -0.85     | -0.92           | -0.69          | -0.74     | -0.88           | -0.78          |
| $^{80}\text{Y}(p, \gamma)^{81}\text{Zr}$    | $^{80}\text{Sr}$  | -0.66     | -0.59           | ...            | -0.83     | -0.81           | -0.54          | ...       | ...             | ...            |
| $^{81}\text{Y}(p, \gamma)^{82}\text{Zr}$    | $^{81}\text{Rb}$  | ...       | ...             | ...            | -0.64     | ...             | ...            | ...       | ...             | ...            |
| $^{81}\text{Zr}(p, \gamma)^{82}\text{Nb}$   | $^{81}\text{Rb}$  | -0.81     | -0.94           | -0.73          | -0.53     | -0.76           | -0.54          | -0.56     | -0.77           | -0.60          |
| $^{82}\text{Zr}(p, \gamma)^{83}\text{Nb}$   | $^{82}\text{Sr}$  | -0.93     | -0.96           | -0.76          | -0.90     | -0.94           | -0.69          | -0.65     | -0.81           | -0.63          |
| $^{83}\text{Zr}(p, \gamma)^{84}\text{Nb}$   | $^{83}\text{Sr}$  | ...       | ...             | ...            | -0.70     | -0.79           | ...            | ...       | ...             | ...            |
| $^{84}\text{Zr}(p, \gamma)^{85}\text{Nb}$   | $^{84}\text{Sr}$  | ...       | ...             | ...            | -0.55     | -0.55           | ...            | ...       | ...             | ...            |
| $^{83}\text{Nb}(p, \gamma)^{84}\text{Mo}$   | $^{83}\text{Sr}$  | -0.67     | -0.74           | -0.57          | ...       | ...             | ...            | -0.58     | -0.77           | -0.62          |
| $^{84}\text{Nb}(p, \gamma)^{85}\text{Mo}$   | $^{84}\text{Sr}$  | -0.77     | -0.85           | -0.63          | -0.61     | -0.70           | ...            | ...       | ...             | ...            |
| $^{85}\text{Nb}(p, \gamma)^{86}\text{Mo}$   | $^{85}\text{Y}$   | -0.70     | -0.79           | -0.56          | -0.79     | -0.86           | -0.56          | ...       | ...             | ...            |
| $^{90}\text{Nb}(p, \gamma)^{91}\text{Mo}$   | $^{90}\text{Nb}$  | ...       | ...             | ...            | -0.56     | -0.59           | ...            | ...       | ...             | ...            |
| $^{85}\text{Mo}(p, \gamma)^{86}\text{Tc}$   | $^{85}\text{Y}$   | ...       | ...             | ...            | ...       | ...             | ...            | ...       | -0.51           | ...            |
| $^{86}\text{Mo}(p, \gamma)^{87}\text{Tc}$   | $^{86}\text{Zr}$  | -0.75     | -0.87           | -0.63          | -0.56     | -0.68           | ...            | ...       | -0.68           | ...            |
| $^{87}\text{Mo}(p, \gamma)^{88}\text{Tc}$   | $^{87}\text{Zr}$  | -0.75     | -0.84           | -0.59          | -0.66     | -0.73           | -0.51          | ...       | ...             | ...            |
| $^{88}\text{Mo}(p, \gamma)^{89}\text{Tc}$   | $^{88}\text{Zr}$  | -0.54     | -0.63           | ...            | -0.77     | -0.86           | -0.54          | ...       | ...             | ...            |
| $^{90}\text{Mo}(p, \gamma)^{91}\text{Tc}$   | $^{90}\text{Nb}$  | ...       | ...             | ...            | -0.50     | -0.54           | ...            | ...       | ...             | ...            |
|   | $^{90}\text{Mo}$  | ...       | ...             | ...            | -0.58     | -0.69           | ...            | ...       | ...             | ...            |
| $^{88}\text{Tc}(p, \gamma)^{89}\text{Ru}$   | $^{88}\text{Zr}$  | -0.55     | -0.58           | ...            | ...       | ...             | ...            | ...       | -0.58           | ...            |
| $^{89}\text{Tc}(p, \gamma)^{90}\text{Ru}$   | $^{89}\text{Nb}$  | -0.75     | -0.83           | -0.62          | -0.62     | -0.62           | ...            | ...       | ...             | ...            |
| $^{91}\text{Tc}(p, \gamma)^{92}\text{Ru}$   | $^{91}\text{Nb}$  | -0.54     | -0.65           | ...            | -0.74     | -0.82           | -0.53          | ...       | ...             | ...            |
| $^{90}\text{Ru}(p, \gamma)^{91}\text{Rh}$   | $^{90}\text{Mo}$  | -0.62     | -0.67           | ...            | ...       | ...             | ...            | ...       | -0.61           | ...            |
| $^{92}\text{Ru}(p, \gamma)^{93}\text{Rh}$   | $^{92}\text{Mo}$  | -0.74     | -0.80           | -0.57          | -0.78     | -0.79           | -0.52          | ...       | ...             | ...            |
| $^{93}\text{Ru}(p, \gamma)^{94}\text{Rh}$   | $^{93}\text{Tc}$  | ...       | ...             | ...            | -0.51     | -0.54           | ...            | ...       | ...             | ...            |
| $^{93}\text{Rh}(p, \gamma)^{94}\text{Pd}$   | $^{93}\text{Tc}$  | -0.66     | -0.67           | -0.52          | -0.52     | ...             | ...            | ...       | ...             | ...            |
| $^{94}\text{Rh}(p, \gamma)^{95}\text{Pd}$   | $^{94}\text{Tc}$  | -0.56     | -0.64           | ...            | -0.65     | -0.69           | ...            | ...       | ...             | ...            |
| $^{95}\text{Rh}(p, \gamma)^{96}\text{Pd}$   | $^{95}\text{Ru}$  | -0.55     | -0.68           | ...            | -0.69     | -0.75           | -0.52          | ...       | ...             | ...            |
| $^{96}\text{Pd}(p, \gamma)^{97}\text{Ag}$   | $^{96}\text{Ru}$  | ...       | -0.69           | -0.50          | -0.61     | -0.68           | -0.52          | ...       | ...             | ...            |
| $^{97}\text{Ag}(p, \gamma)^{98}\text{Cd}$   | $^{97}\text{Ru}$  | -0.58     | -0.71           | -0.51          | -0.61     | -0.65           | -0.51          | ...       | ...             | ...            |
| $^{98}\text{Ag}(p, \gamma)^{99}\text{Cd}$   | $^{98}\text{Ru}$  | -0.50     | -0.61           | ...            | -0.61     | -0.66           | ...            | ...       | ...             | ...            |
| $^{99}\text{Ag}(p, \gamma)^{100}\text{Cd}$  | $^{99}\text{Rh}$  | ...       | ...             | ...            | -0.53     | -0.51           | ...            | ...       | ...             | ...            |
| $^{99}\text{Cd}(p, \gamma)^{100}\text{In}$  | $^{99}\text{Rh}$  | ...       | -0.58           | ...            | -0.53     | -0.63           | ...            | ...       | ...             | ...            |
| $^{100}\text{Cd}(p, \gamma)^{101}\text{In}$ | $^{100}\text{Pd}$ | ...       | ...             | ...            | -0.64     | ...             | ...            | ...       | ...             | ...            |
| $^{101}\text{In}(p, \gamma)^{102}\text{Sn}$ | $^{101}\text{Pd}$ | ...       | ...             | ...            | -0.50     | -0.57           | ...            | ...       | ...             | ...            |
| $^{102}\text{In}(p, \gamma)^{103}\text{Sn}$ | $^{102}\text{Pd}$ | ...       | -0.57           | ...            | -0.75     | -0.79           | -0.55          | ...       | ...             | ...            |
| $^{103}\text{In}(p, \gamma)^{104}\text{Sn}$ | $^{103}\text{Pd}$ | ...       | ...             | ...            | -0.66     | -0.76           | ...            | ...       | ...             | ...            |
|   | $^{103}\text{Ag}$ | ...       | -0.50           | ...            | -0.88     | -0.88           | -0.66          | ...       | ...             | ...            |

Table 1 continued

**Table 1** (*continued*)

| Reaction                                    | Isotope           | Model K04 |                 |                | Model S01 |                 |                | Model S16 |                 |                |
|---|-------------------|-----------|-----------------|----------------|-----------|-----------------|----------------|-----------|-----------------|----------------|
|   |                   | STARLIB   | $\sigma = 1.15$ | $\sigma = 2.3$ | STARLIB   | $\sigma = 1.15$ | $\sigma = 2.3$ | STARLIB   | $\sigma = 1.15$ | $\sigma = 2.3$ |
| $^{104}\text{In}(p, \gamma)^{105}\text{Sn}$ | $^{104}\text{Ag}$ | ...       | 0.60            | ...            | ...       | ...             | ...            | ...       | ...             | ...            |
|   | $^{104}\text{Pd}$ | ...       | ...             | ...            | -0.58     | -0.72           | ...            | ...       | ...             | ...            |
|   | $^{104}\text{Ag}$ | ...       | ...             | ...            | -0.79     | -0.80           | -0.57          | ...       | ...             | ...            |
|   | $^{105}\text{Ag}$ | 0.54      | 0.68            | ...            | ...       | 0.58            | ...            | ...       | ...             | ...            |
|   | $^{106}\text{Cd}$ | ...       | 0.53            | ...            | ...       | ...             | ...            | ...       | ...             | ...            |
| $^{105}\text{In}(p, \gamma)^{106}\text{Sn}$ | $^{105}\text{Ag}$ | ...       | ...             | ...            | -0.59     | -0.57           | ...            | ...       | ...             | ...            |
|   | $^{106}\text{Cd}$ | ...       | ...             | ...            | ...       | 0.54            | ...            | ...       | ...             | ...            |
| $^{106}\text{Sn}(p, \gamma)^{107}\text{Sb}$ | $^{106}\text{Cd}$ | ...       | ...             | ...            | -0.51     | ...             | ...            | ...       | ...             | ...            |
|   | $^{107}\text{Cd}$ | ...       | 0.59            | ...            | 0.52      | 0.67            | ...            | ...       | ...             | ...            |
| $^{107}\text{Sn}(p, \gamma)^{108}\text{Sb}$ | $^{108}\text{Cd}$ | ...       | 0.59            | ...            | ...       | 0.66            | ...            | ...       | ...             | ...            |
| $^{108}\text{Sn}(p, \gamma)^{109}\text{Sb}$ | $^{109}\text{In}$ | ...       | ...             | ...            | ...       | 0.58            | ...            | ...       | ...             | ...            |

**Table 2.** Abundance uncertainties of Models K04, S01, and S16 for the temperature-dependent (STARLIB: 84<sup>th</sup>/16<sup>th</sup> percentile ratio) and -independent Monte Carlo simulations ( $\sigma = 2.3$ : 84<sup>th</sup>/16<sup>th</sup> percentile ratio,  $\sigma = 1.15$ : 97.5<sup>th</sup>/2.5<sup>th</sup> percentile ratio). Abundance uncertainties are listed only with isotopic baseline abundances  $X_{\text{base}} \geq 10^{-6}$  and uncertainties equal to or exceeding a factor of 2.

| Isotope          | Model K04 |                 |                | Model S01 |                 |                | Model S16 |                 |                |
|------------------|-----------|-----------------|----------------|-----------|-----------------|----------------|-----------|-----------------|----------------|
|                  | STARLIB   | $\sigma = 1.15$ | $\sigma = 2.3$ | STARLIB   | $\sigma = 1.15$ | $\sigma = 2.3$ | STARLIB   | $\sigma = 1.15$ | $\sigma = 2.3$ |
| $^1\text{H}$     | ...       | 2.2             | 4.8            | 2.6       | 4708.6          | $> 10^4$       | ...       | ...             | ...            |
| $^{14}\text{N}$  | 107.6     | ...             | ...            | 131.2     | 752.8           | $> 10^4$       | 3.5       | ...             | 2.0            |
| $^{15}\text{N}$  | 6.7       | 374.8           | 2411.2         | 6.6       | 1840.9          | $> 10^4$       | 2.7       | 8.8             | 10.0           |
| $^{18}\text{F}$  | 2.5       | 41.0            | 235.7          | ...       | 95.9            | $> 10^4$       | 26.8      | 38.5            | 38.2           |
| $^{20}\text{Ne}$ | ...       | ...             | ...            | ...       | ...             | ...            | ...       | 13.4            | 14.5           |
| $^{21}\text{Ne}$ | ...       | 40.1            | 142.7          | ...       | 36.7            | $> 10^4$       | ...       | 13.4            | 16.5           |
| $^{22}\text{Na}$ | 11.6      | 41.2            | 109.4          | 7.8       | ...             | ...            | 6.9       | 60.1            | 76.5           |
| $^{23}\text{Na}$ | ...       | ...             | ...            | ...       | 2.0             | $> 10^4$       | 5.9       | 17.9            | 24.2           |
| $^{24}\text{Mg}$ | ...       | ...             | ...            | ...       | ...             | 10.0           | 6.1       | 17.2            | 18.5           |
| $^{25}\text{Mg}$ | ...       | ...             | ...            | ...       | ...             | 2.1            | ...       | 54.4            | 54.3           |
| $^{27}\text{Al}$ | ...       | 4.3             | 5.0            | ...       | 6.2             | 23.3           | 5.9       | 12.8            | 13.8           |
| $^{28}\text{Si}$ | ...       | ...             | ...            | ...       | ...             | 26.9           | 5.9       | 12.7            | 13.3           |
| $^{29}\text{Si}$ | ...       | ...             | ...            | ...       | ...             | 5.2            | 5.9       | 12.6            | 13.3           |
| $^{30}\text{Si}$ | ...       | 3.0             | 3.9            | ...       | 4.2             | 17.2           | 6.7       | 30.1            | 32.0           |
| $^{31}\text{P}$  | ...       | 2.2             | 2.1            | ...       | 3.7             | 2.9            | 6.1       | 28.8            | 29.0           |
| $^{32}\text{S}$  | ...       | ...             | ...            | ...       | ...             | 57.5           | 6.0       | 16.1            | 17.2           |

**Table 2** *continued*

**Table 2** (*continued*)

| Isotope          | Model K04 |                 |                | Model S01 |                 |                | Model S16 |                 |                |
|------------------|-----------|-----------------|----------------|-----------|-----------------|----------------|-----------|-----------------|----------------|
|                  | STARLIB   | $\sigma = 1.15$ | $\sigma = 2.3$ | STARLIB   | $\sigma = 1.15$ | $\sigma = 2.3$ | STARLIB   | $\sigma = 1.15$ | $\sigma = 2.3$ |
| <sup>33</sup> S  | ...       | ...             | ...            | ...       | ...             | ...            | 6.0       | 13.7            | 18.1           |
| <sup>34</sup> S  | ...       | 4.0             | 3.5            | ...       | 3.4             | 4.8            | 5.9       | 12.1            | 12.3           |
| <sup>35</sup> Cl | ...       | 11.1            | 12.4           | ...       | 38.3            | 128.6          | ...       | ...             | ...            |
| <sup>36</sup> Ar | ...       | ...             | ...            | ...       | ...             | 36.9           | 6.0       | 13.8            | 13.6           |
| <sup>37</sup> Ar | ...       | ...             | ...            | ...       | ...             | ...            | 8.3       | 22.2            | 27.6           |
| <sup>38</sup> Ar | ...       | ...             | ...            | ...       | ...             | ...            | 6.1       | 11.9            | 12.4           |
| <sup>39</sup> K  | 2.8       | 89.6            | 328.7          | 4.0       | ...             | ...            | 6.4       | 40.1            | 52.3           |
| <sup>40</sup> Ca | ...       | ...             | ...            | ...       | 18.8            | 1670.7         | 7.1       | 140.3           | 202.3          |
| <sup>41</sup> Ca | ...       | ...             | ...            | ...       | ...             | 2.1            | 31.2      | 59.8            | 54.3           |
| <sup>42</sup> Ca | 2.7       | 2.7             | 2.9            | 2.1       | 2.7             | 3.4            | 8.4       | 13.9            | 14.0           |
| <sup>43</sup> Sc | ...       | ...             | ...            | ...       | ...             | ...            | 56.6      | 100.8           | 105.2          |
| <sup>44</sup> Ti | 6.6       | 6.9             | 5.8            | ...       | 30.9            | 233.8          | 25.8      | 43.3            | 50.1           |
| <sup>45</sup> Ti | 19.3      | 10.4            | 9.5            | ...       | 13.5            | 16.7           | 28.4      | 20.6            | 23.3           |
| <sup>46</sup> Ti | 3.0       | 10.8            | 12.4           | 4.4       | 12.7            | 13.8           | 12.5      | 33.5            | 29.2           |
| <sup>47</sup> Ti | ...       | 2.7             | 4.5            | ...       | ...             | ...            | 23.8      | 35.9            | 40.5           |
| <sup>49</sup> V  | 4.2       | 3.6             | 4.6            | 3.4       | 4.0             | 8.0            | 29.9      | 93.4            | 62.5           |
| <sup>48</sup> Cr | ...       | ...             | 2.7            | ...       | 3.7             | 23.3           | 109.9     | 196.5           | 224.2          |
| <sup>50</sup> Cr | 29.7      | 13.8            | 15.7           | 24.8      | 11.0            | 14.2           | 28.9      | 84.0            | 61.4           |
| <sup>51</sup> Cr | 29.1      | ...             | ...            | 32.9      | ...             | ...            | 127.2     | 245.1           | 154.3          |
| <sup>52</sup> Mn | ...       | ...             | ...            | ...       | ...             | ...            | ...       | 197.9           | 108.5          |
| <sup>53</sup> Mn | ...       | ...             | 2.1            | 3.3       | 3.1             | 4.8            | 65.3      | 64.5            | 62.9           |
| <sup>52</sup> Fe | 3.3       | 2.3             | 8.7            | 10.0      | 44.0            | 181.6          | 123.8     | 81.6            | 55.3           |
| <sup>54</sup> Fe | ...       | ...             | ...            | ...       | ...             | 3.2            | 70.1      | 64.4            | 62.7           |
| <sup>55</sup> Co | 23.1      | 26.5            | 53.1           | 24.0      | ...             | ...            | 82.2      | 38.5            | 49.1           |
| <sup>56</sup> Ni | 12.3      | 11.7            | 69.1           | 27.2      | 129.1           | 1172.5         | 277.3     | 175.0           | 397.1          |
| <sup>57</sup> Ni | 3.6       | 3.1             | 5.7            | 9.0       | 9.4             | 19.1           | 29.0      | 17.2            | 22.2           |
| <sup>58</sup> Ni | ...       | ...             | ...            | 2.9       | 2.2             | 4.4            | 24.0      | 28.6            | 30.6           |
| <sup>59</sup> Ni | ...       | ...             | 2.9            | ...       | 4.2             | 4.4            | 32.4      | 29.7            | 32.4           |
| <sup>60</sup> Ni | 47.0      | 94.7            | 250.4          | 34.9      | 248.3           | 313.6          | 24.8      | 44.2            | 44.9           |
| <sup>61</sup> Ni | ...       | ...             | ...            | ...       | ...             | ...            | 78.8      | ...             | ...            |
| <sup>62</sup> Ni | ...       | ...             | ...            | ...       | ...             | ...            | 37.4      | 60.2            | 58.4           |
| <sup>61</sup> Cu | 51.8      | 61.5            | 94.1           | 40.6      | 117.9           | 410.8          | 45.1      | 70.6            | 81.6           |
| <sup>63</sup> Cu | 2.9       | 3.3             | 4.6            | 7.7       | 11.6            | 11.6           | 36.0      | 21.8            | 24.3           |
| <sup>62</sup> Zn | 2.0       | ...             | ...            | 3.2       | 2.3             | 4.6            | 39.8      | 85.4            | 80.9           |
| <sup>64</sup> Zn | 11.7      | 10.0            | 11.5           | 2.4       | 2.2             | 4.5            | 3.1       | ...             | ...            |
| <sup>65</sup> Zn | 79.7      | 130.4           | 120.5          | 102.6     | 139.2           | 229.0          | 12.7      | 11.6            | 12.6           |
| <sup>66</sup> Ga | ...       | ...             | ...            | ...       | ...             | ...            | 15.7      | 16.0            | 16.6           |

**Table 2** *continued*

**Table 2** (*continued*)

| Isotope           | Model K04 |                 |                | Model S01 |                 |                | Model S16 |                 |                |
|-------------------|-----------|-----------------|----------------|-----------|-----------------|----------------|-----------|-----------------|----------------|
|                   | STARLIB   | $\sigma = 1.15$ | $\sigma = 2.3$ | STARLIB   | $\sigma = 1.15$ | $\sigma = 2.3$ | STARLIB   | $\sigma = 1.15$ | $\sigma = 2.3$ |
| <sup>67</sup> Ga  | 15.4      | 30.8            | 27.1           | 29.6      | 57.3            | 61.6           | 35.1      | 28.9            | 34.3           |
| <sup>66</sup> Ge  | 23.1      | 37.6            | 32.3           | 19.6      | 37.0            | 47.3           | 20.1      | 20.1            | 20.7           |
| <sup>68</sup> Ge  | ...       | ...             | ...            | ...       | ...             | 3.7            | 4.8       | 2.3             | 2.7            |
| <sup>69</sup> Ge  | 94.2      | 95.6            | 116.7          | 88.0      | 116.0           | 106.5          | 22.8      | 14.7            | 17.5           |
| <sup>70</sup> Ge  | 14.6      | 21.4            | 17.6           | 33.5      | 40.1            | 42.4           | 27.2      | 20.0            | 23.3           |
| <sup>71</sup> As  | 26.2      | 33.8            | 36.6           | 58.6      | 78.9            | 83.3           | 48.1      | 36.2            | 43.8           |
| <sup>72</sup> Se  | ...       | ...             | ...            | ...       | ...             | 3.3            | 7.1       | 3.2             | 4.1            |
| <sup>73</sup> Se  | 86.3      | 86.5            | 144.1          | 59.3      | 76.7            | 94.7           | 27.2      | 16.2            | 20.4           |
| <sup>74</sup> Se  | 24.4      | 22.7            | 28.5           | 54.6      | 50.8            | 60.7           | 36.4      | 26.1            | 29.2           |
| <sup>75</sup> Br  | 52.2      | 56.7            | 70.1           | 49.5      | 66.3            | 93.3           | 62.4      | 43.2            | 54.3           |
| <sup>76</sup> Kr  | ...       | ...             | 2.2            | 3.8       | 3.0             | 5.6            | 9.7       | 4.1             | 5.8            |
| <sup>77</sup> Kr  | 45.7      | 55.7            | 103.3          | 18.9      | 31.4            | 45.1           | 27.9      | 18.1            | 21.9           |
| <sup>78</sup> Kr  | 53.3      | 50.1            | 70.4           | 48.8      | 64.3            | 91.9           | 42.3      | 26.7            | 31.9           |
| <sup>79</sup> Kr  | 42.5      | 51.4            | 95.2           | 19.9      | 31.7            | 50.3           | 59.1      | 40.6            | 52.7           |
| <sup>81</sup> Rb  | 18.5      | 25.6            | 56.4           | 11.4      | 15.3            | 25.7           | 34.9      | 21.5            | 28.3           |
| <sup>80</sup> Sr  | 4.1       | 2.8             | 4.7            | 8.9       | 7.4             | 11.4           | 14.3      | 5.6             | 8.6            |
| <sup>82</sup> Sr  | 41.7      | 35.3            | 79.3           | 21.9      | 21.9            | 38.2           | 51.1      | 22.7            | 31.1           |
| <sup>83</sup> Sr  | 11.9      | 14.4            | 26.0           | 10.6      | 13.6            | 76.6           | 42.4      | 25.6            | 33.0           |
| <sup>84</sup> Sr  | 9.1       | 10.2            | 15.5           | 9.8       | 12.6            | 16.0           | 23.4      | 10.6            | 16.4           |
| <sup>85</sup> Y   | 10.5      | 8.8             | 18.5           | 12.3      | 12.6            | 31.0           | 31.1      | 13.9            | 21.9           |
| <sup>86</sup> Zr  | 8.9       | 10.8            | 17.6           | 6.8       | 9.0             | 13.7           | 30.5      | 16.7            | 22.7           |
| <sup>87</sup> Zr  | 12.1      | 10.4            | 21.2           | 10.6      | 12.2            | 19.8           | 41.5      | 18.6            | 29.2           |
| <sup>88</sup> Zr  | 11.0      | 12.0            | 22.4           | 13.7      | 15.1            | 24.0           | 41.7      | 20.4            | 29.8           |
| <sup>89</sup> Nb  | 14.3      | 14.0            | 31.1           | 12.5      | 15.1            | 38.2           | 46.3      | 20.0            | 33.6           |
| <sup>90</sup> Nb  | ...       | ...             | ...            | 76.4      | 110.6           | 216.3          | ...       | ...             | ...            |
| <sup>91</sup> Nb  | 10.7      | 10.1            | 21.6           | 16.5      | 18.3            | 30.9           | 47.4      | 21.2            | 34.5           |
| <sup>90</sup> Mo  | 10.7      | 10.2            | 24.1           | 10.8      | 11.4            | 17.8           | 58.2      | 28.8            | 44.0           |
| <sup>92</sup> Mo  | 16.1      | 13.7            | 32.9           | 17.3      | 17.2            | 34.3           | 54.9      | 25.9            | 40.5           |
| <sup>93</sup> Mo  | ...       | ...             | ...            | 75.4      | ...             | ...            | ...       | ...             | ...            |
| <sup>93</sup> Tc  | 15.0      | 15.3            | 35.3           | 12.0      | 13.9            | 22.7           | 72.1      | 35.4            | 58.6           |
| <sup>94</sup> Tc  | 12.2      | 12.2            | 28.1           | 11.6      | 13.1            | 21.8           | 79.0      | 37.2            | 63.5           |
| <sup>95</sup> Ru  | 13.8      | 14.3            | 32.7           | 15.4      | 18.0            | 31.8           | 90.2      | 40.1            | 69.9           |
| <sup>96</sup> Ru  | 9.6       | 13.7            | 40.8           | 7.2       | 13.3            | 25.4           | 92.0      | 44.4            | 77.1           |
| <sup>97</sup> Ru  | 16.6      | 17.5            | 45.2           | 11.8      | 14.6            | 25.9           | ...       | 70.6            | 117.8          |
| <sup>98</sup> Ru  | 16.2      | 12.9            | 34.1           | 13.8      | 16.9            | 34.4           | ...       | ...             | ...            |
| <sup>99</sup> Rh  | 14.1      | 13.9            | 39.0           | 12.0      | 14.9            | 26.9           | ...       | ...             | ...            |
| <sup>100</sup> Pd | 11.2      | 7.4             | 25.0           | 5.9       | 5.0             | 9.8            | ...       | ...             | ...            |

**Table 2** *continued*



**Table 2** (*continued*)

| Isotope           | Model K04 |                 |                | Model S01 |                 |                | Model S16 |                 |                |
|-------------------|-----------|-----------------|----------------|-----------|-----------------|----------------|-----------|-----------------|----------------|
|                   | STARLIB   | $\sigma = 1.15$ | $\sigma = 2.3$ | STARLIB   | $\sigma = 1.15$ | $\sigma = 2.3$ | STARLIB   | $\sigma = 1.15$ | $\sigma = 2.3$ |
| <sup>101</sup> Pd | 17.2      | 15.2            | 44.7           | 9.4       | 11.7            | 19.9           | ...       | ...             | ...            |
| <sup>102</sup> Pd | 20.7      | 19.3            | 57.4           | 10.8      | 15.1            | 24.2           | ...       | ...             | ...            |
| <sup>103</sup> Pd | ...       | ...             | ...            | 25.2      | 19.3            | 71.5           | ...       | ...             | ...            |
| <sup>104</sup> Pd | ...       | ...             | ...            | 12.8      | 7.4             | 29.2           | ...       | ...             | ...            |
| <sup>103</sup> Ag | 24.1      | 18.2            | 72.7           | 11.2      | 12.7            | 37.3           | ...       | ...             | ...            |
| <sup>104</sup> Ag | 25.4      | 19.9            | 85.5           | 3.6       | 3.7             | 8.9            | ...       | ...             | ...            |
| <sup>105</sup> Ag | 39.7      | 36.8            | 161.1          | 3.3       | 3.2             | 10.5           | ...       | ...             | ...            |
| <sup>106</sup> Cd | 51.2      | 47.7            | 266.6          | 5.2       | 5.6             | 26.0           | ...       | ...             | ...            |
| <sup>107</sup> Cd | 79.9      | 90.6            | 559.3          | 14.7      | 20.3            | 137.7          | ...       | ...             | ...            |
| <sup>108</sup> Cd | 107.0     | 174.2           | 913.1          | 20.8      | 54.9            | 1086.9         | ...       | ...             | ...            |
| <sup>109</sup> In | ...       | ...             | ...            | 30.4      | 118.3           | 7206.2         | ...       | ...             | ...            |
| <sup>110</sup> In | ...       | ...             | ...            | 24.9      | ...             | ...            | ...       | ...             | ...            |
| <sup>111</sup> In | ...       | ...             | ...            | 35.5      | 123.5           | 4761.2         | ...       | ...             | ...            |
| <sup>110</sup> Sn | ...       | ...             | ...            | 22.8      | 89.4            | 4239.4         | ...       | ...             | ...            |
| <sup>112</sup> Sn | ...       | ...             | ...            | 44.9      | 140.5           | 2062.5         | ...       | ...             | ...            |
| <sup>113</sup> Sn | ...       | ...             | ...            | 62.5      | 259.3           | 7196.7         | ...       | ...             | ...            |
| <sup>114</sup> Sn | ...       | ...             | ...            | 70.3      | ...             | ...            | ...       | ...             | ...            |
| <sup>115</sup> Sn | ...       | ...             | ...            | 73.9      | ...             | ...            | ...       | ...             | ...            |
| <sup>116</sup> Te | ...       | ...             | ...            | 72.7      | ...             | ...            | ...       | ...             | ...            |
| <sup>117</sup> Te | ...       | ...             | ...            | 83.9      | ...             | ...            | ...       | ...             | ...            |
| <sup>118</sup> Te | ...       | ...             | ...            | 89.7      | ...             | ...            | ...       | ...             | ...            |

## REFERENCES

- Angulo, C., Arnould, M., Rayet, M., et al. 1999, Nuclear Physics A, 656, 3, doi: [10.1016/S0375-9474\(99\)00030-5](https://doi.org/10.1016/S0375-9474(99)00030-5)
- Bliss, J., Arcones, A., Montes, F., & Pereira, J. 2020, Physical Review C, 101, 055807, doi: [10.1103/PhysRevC.101.055807](https://doi.org/10.1103/PhysRevC.101.055807)
- Cescutti, G., Hirschi, R., Nishimura, N., et al. 2018, Monthly Notices of the Royal Astronomical Society, 478, 4101, doi: [10.1093/MNRAS/STY1185](https://doi.org/10.1093/MNRAS/STY1185)
- Cyburt, R. H., Amthor, A. M., Heger, A., et al. 2016, The Astrophysical Journal, 830, 55, doi: [10.3847/0004-637X/830/2/55](https://doi.org/10.3847/0004-637X/830/2/55)
- Cyburt, R. H., Amthor, A. M., Ferguson, R., et al. 2010, The Astrophysical Journal Supplement Series, 189, 240, doi: [10.1088/0067-0049/189/1/240](https://doi.org/10.1088/0067-0049/189/1/240)
- Denissenkov, P. A., Herwig, F., Perdikakis, G., & Schatz, H. 2021, Monthly Notices of the Royal Astronomical Society, 503, 3913, doi: [10.1093/MNRAS/STAB772](https://doi.org/10.1093/MNRAS/STAB772)
- Fields, C. E., Farmer, R., Petermann, I., Iliadis, C., & Timmes, F. X. 2016, The Astrophysical Journal, 823, 46, doi: [10.3847/0004-637X/823/1/46](https://doi.org/10.3847/0004-637X/823/1/46)
- Fields, C. E., Timmes, F. X., Farmer, R., et al. 2018, The Astrophysical Journal Supplement Series, 234, 19, doi: [10.3847/1538-4365/AAA29B](https://doi.org/10.3847/1538-4365/AAA29B)
- Fisker, J. L., Schatz, H., & Thielemann, F. 2008, The Astrophysical Journal Supplement Series, 174, 261, doi: [10.1086/521104](https://doi.org/10.1086/521104)
- Grevesse, N., Sauval, A. J., Grevesse, N., & Sauval, A. J. 1998, SSRv, 85, 161, doi: [10.1023/A:1005161325181](https://doi.org/10.1023/A:1005161325181)
- Hansen, C. J., van Horn, H. M., Hansen, C. J., & van Horn, H. M. 1975, ApJ, 195, 735, doi: [10.1086/153375](https://doi.org/10.1086/153375)

- Harris, C. R., Millman, K. J., van der Walt, S. J., et al. 2020, *Nature*, 585, 357, doi: [10.1038/s41586-020-2649-2](https://doi.org/10.1038/s41586-020-2649-2)
- Hunter, J. D. 2007, *Computing in Science & Engineering*, 9, 90, doi: [10.1109/MCSE.2007.55](https://doi.org/10.1109/MCSE.2007.55)
- Iliadis, C., & Coc, A. 2020, *The Astrophysical Journal*, 901, 127, doi: [10.3847/1538-4357/ABB1A3](https://doi.org/10.3847/1538-4357/ABB1A3)
- Joss, P. C. 1977, *Nature*, 270, 310, doi: [10.1038/270310A0;KWRD](https://doi.org/10.1038/270310A0;KWRD)
- José, J., Moreno, F., Parikh, A., & Iliadis, C. 2010, *The Astrophysical Journal Supplement Series*, 189, 204, doi: [10.1088/0067-0049/189/1/204](https://doi.org/10.1088/0067-0049/189/1/204)
- Kluyver, T., Ragan-Kelley, B., Pérez, F., et al. 2016, in *Positioning and Power in Academic Publishing: Players, Agents and Agendas*, ed. F. Loizides & B. Schmidt, IOS Press, 87 – 90
- Koike, O., Hashimoto, M., Kuromizu, R., & Fujimoto, S. 2004, *The Astrophysical Journal*, 603, 242, doi: [10.1086/381354](https://doi.org/10.1086/381354)
- Lam, Y. H., Heger, A., Johnston, Z., & Goodwin, A. J. 2022a, *EPJ Web of Conferences*, 260, 11028, doi: [10.1051/EPJCONF/202226011028](https://doi.org/10.1051/EPJCONF/202226011028)
- Lam, Y. H., Liu, Z. X., Heger, A., et al. 2022b, *The Astrophysical Journal*, 929, 72, doi: [10.3847/1538-4357/AC4D8B](https://doi.org/10.3847/1538-4357/AC4D8B)
- Lam, Y. H., Lu, N., Heger, A., et al. 2022c, *The Astrophysical Journal*, 929, 73, doi: [10.3847/1538-4357/AC4D89](https://doi.org/10.3847/1538-4357/AC4D89)
- Lam, Y. H., , Lu, N., et al. 2025, *The Astrophysical Journal*, 993, 121, doi: [10.3847/1538-4357/ADE055](https://doi.org/10.3847/1538-4357/ADE055)
- Lippuner, J., & Roberts, L. F. 2017, *The Astrophysical Journal Supplement Series*, 233, 18, doi: [10.3847/1538-4365/AA94CB](https://doi.org/10.3847/1538-4365/AA94CB)
- Longland, R. 2012, *Astronomy & Astrophysics*, 548, A30, doi: [10.1051/0004-6361/201220386](https://doi.org/10.1051/0004-6361/201220386)
- Longland, R., Iliadis, C., Champagne, A. E., et al. 2010, *Nuclear Physics A*, 841, 1, doi: [10.1016/J.NUCLPHYSA.2010.04.008](https://doi.org/10.1016/J.NUCLPHYSA.2010.04.008)
- Meyer, B. S., Adams, D. C., Meyer, B. S., & Adams, D. C. 2007, *M&PSA*, 42, 5215. <https://ui.adsabs.harvard.edu/abs/2007M&PSA.42.5215M/abstract>
- Moreno, F., & José, J. 2009, PhD thesis, Universitat Politècnica de Catalunya, doi: [10.5821/DISSERTATION-2117-93905](https://doi.org/10.5821/DISSERTATION-2117-93905)
- Mumpower, M. R., Surman, R., McLaughlin, G. C., & Aprahamian, A. 2016, *Progress in Particle and Nuclear Physics*, 86, 86, doi: [10.1016/J.PPNP.2015.09.001](https://doi.org/10.1016/J.PPNP.2015.09.001)
- Nishimura, N., Rauscher, T., Hirschi, R., et al. 2019, *Monthly Notices of the Royal Astronomical Society*, 489, 1379, doi: [10.1093/MNRAS/STZ2104](https://doi.org/10.1093/MNRAS/STZ2104)
- Parikh, A., José, J., Moreno, F., & Iliadis, C. 2008, *The Astrophysical Journal Supplement Series*, 178, 110, doi: [10.1086/589879](https://doi.org/10.1086/589879)
- Parikh, A., José, J., Sala, G., & Iliadis, C. 2013, *Progress in Particle and Nuclear Physics*, 69, 225, doi: [10.1016/J.PPNP.2012.11.002](https://doi.org/10.1016/J.PPNP.2012.11.002)
- Pedregosa, F., Varoquaux, G., Gramfort, A., et al. 2011, *Journal of Machine Learning Research*, 12, 2825
- Pérez, F., & Granger, B. E. 2007, *Computing in Science and Engineering*, 9, 21, doi: [10.1109/MCSE.2007.53](https://doi.org/10.1109/MCSE.2007.53)
- Psaltis, A., Arcones, A., Montes, F., et al. 2022, *The Astrophysical Journal*, 935, 27, doi: [10.3847/1538-4357/AC7DA7](https://doi.org/10.3847/1538-4357/AC7DA7)
- Psaltis, A., José, J., Longland, R., & Iliadis, C. 2025, *The Astrophysical Journal*, 987, 88, doi: [10.3847/1538-4357/addfd5](https://doi.org/10.3847/1538-4357/addfd5)
- Rauscher, T., Nishimura, N., Hirschi, R., et al. 2016, *Monthly Notices of the Royal Astronomical Society*, 463, 4153, doi: [10.1093/MNRAS/STW2266](https://doi.org/10.1093/MNRAS/STW2266)
- Reichert, M., Winteler, C., Korobkin, O., et al. 2023, *The Astrophysical Journal Supplement Series*, 268, 66, doi: [10.3847/1538-4365/acf033](https://doi.org/10.3847/1538-4365/acf033)
- Roberts, L. F., Hix, W. R., Smith, M., & Fisker, J. L. 2006, *International Symposium on Nuclear Astrophysics-Nuclei in the Cosmos-IX*. <http://pos.sissa.it/>
- Sallaska, A. L., Iliadis, C., Champagne, A. E., et al. 2013, *The Astrophysical Journal Supplement Series*, 207, 18, doi: [10.1088/0067-0049/207/1/18](https://doi.org/10.1088/0067-0049/207/1/18)
- Schatz, H. 2006, *International Journal of Mass Spectrometry*, 251, 293, doi: [10.1016/J.IJMS.2006.02.014](https://doi.org/10.1016/J.IJMS.2006.02.014)
- Schatz, H. 2016, *Journal of Physics G: Nuclear and Particle Physics*, 43, 064001, doi: [10.1088/0954-3899/43/6/064001](https://doi.org/10.1088/0954-3899/43/6/064001)
- Schatz, H., Aprahamian, A., Barnard, V., et al. 2001, *Phys. Rev. Lett.*, 86, 3471, doi: [10.1103/PhysRevLett.86.3471](https://doi.org/10.1103/PhysRevLett.86.3471)
- van Wormer, L., Görres, J., Iliadis, C., et al. 1994, *ApJ*, 432, 326, doi: [10.1086/174572](https://doi.org/10.1086/174572)
- Virtanen, P., Gommers, R., Oliphant, T. E., et al. 2020, *Nature Methods*, 17, 261, doi: [10.1038/s41592-019-0686-2](https://doi.org/10.1038/s41592-019-0686-2)
- Wallace, R. K., Woosley, S. E., Wallace, R. K., & Woosley, S. E. 1981, *ApJS*, 45, 389, doi: [10.1086/190717](https://doi.org/10.1086/190717)
- Waskom, M. L. 2021, *Journal of Open Source Software*, 6, 3021, doi: [10.21105/joss.03021](https://doi.org/10.21105/joss.03021)
- Winteler, C., Käppeli, R., Perego, A., et al. 2012, *The Astrophysical Journal Letters*, 750, L22, doi: [10.1088/2041-8205/750/1/L22](https://doi.org/10.1088/2041-8205/750/1/L22)
- Woosley, S. E., & Taam, R. E. 1976, *Nature*, 263, 101, doi: [10.1038/263101A0;KWRD](https://doi.org/10.1038/263101A0;KWRD)
- Woosley, S. E., Heger, A., Cumming, A., et al. 2004, *The Astrophysical Journal Supplement Series*, 151, 75, doi: [10.1086/381533](https://doi.org/10.1086/381533)

Zhang, M., Xu, X., Xing, Y. M., & Hou, S. Q. 2024,  
Physical Review C, 109, 045802,  
doi: [10.1103/PhysRevC.109.045802](https://doi.org/10.1103/PhysRevC.109.045802)

Zhou, X., Wang, M., Zhang, Y. H., et al. 2023, Nature  
Physics, 19, 1091,  
doi: [10.1038/S41567-023-02034-2](https://doi.org/10.1038/S41567-023-02034-2);SUBJMETA